Lawrence Berkeley National Laboratory

Lawrence Berkeley National Laboratory

Title
Shape Optimization of Swimming Sheets

Permalink
https://escholarship.org/uc/item/04q8q067

Authors
Wilkening, J.
Hosoi, A.E.

Publication Date
2005-03-01

Peer reviewed

Shape Optimization of Swimming Sheets

By JON WILKENING[1], AND A. E. HOSOI[2]

[1]Department of Mathematics and Lawrence Berkeley National Laboratory, University of California, Berkeley, CA 94721. This author was supported in part by the U.S. Department of Energy and by the National Science Foundation through grant DMS-0101439.

[2]Hatsopoulos Microfluids Laboratory, Department of Mechanical Engineering, Massachusetts Institute of Technology, 77 Massachusetts Avenue, Cambridge, MA 02139, USA

The swimming behavior of a flexible sheet which moves by propagating deformation waves along its body was first studied by G. I. Taylor in 1951. In addition to being of theoretical interest, this problem serves as a useful model of the locomotion of gastropods and various micro-organisms. Although the mechanics of swimming via wave propagation has been studied extensively, relatively little work has been done to define or describe optimal swimming by this mechanism. We carry out this objective for a sheet that is separated from a rigid substrate by a thin film of viscous Newtonian fluid. Using a lubrication approximation to model the dynamics, we derive the relevant Euler-Lagrange equations to optimize swimming speed and efficiency. The optimization equations are solved numerically using two different schemes: a limited memory BFGS method that uses cubic splines to represent the wave profile, and a multi-shooting Runge-Kutta approach that uses the Levenberg-Marquardt method to vary the parameters of the equations until the constraints are satisfied. The former approach is less efficient but generalizes nicely to the non-lubrication setting. For each optimization problem we obtain a one parameter family of solutions that becomes singular in a self-similar fashion as the parameter approaches a critical value. We explore the validity of the lubrication approximation near this singular limit by monitoring higher order corrections to the zeroth order theory and by comparing the results with finite element solutions of the full Stokes equations.

1. Introduction

Swimming at low Reynolds numbers has long been a topic of interest, particularly in the context of mechanical locomotive strategies of mircoorganisms such as spermatozoa and nematodes. The first study to investigate such swimmers from a hydrodynamical point of view was presented by G. I. Taylor on the motion of a two-dimensional swimming flapping sheet (Taylor 1951), in which Taylor analyzes the swimming speed of such an organism in the limit of low amplitude flapping oscillations. Shortly after Taylor's pioneering work, Hancock (Hancock 1953) proposed an alternate approach, calculating swimming speeds by modeling the swimmer's tail with a distribution of Stokeslets and doublets. As Hancock's approach is more general than Taylor's, he was able to investigate a variety of geometries including both finite and infinite length tails as well as a variety of steady shape disturbances including helical motions and both transverse and longitudinal waves. These theoretical predictions were then successfully compared with experimentally measured swimming velocities of nematodes. Numerous subsequent studies are further discussed in two comprehensive review articles, Lighthill (1976) and Pedley & Kessler (1992). While the mechanics of free low Reynolds number swimmers

has been analyzed extensively, far fewer studies exist in which the optimization of such systems has been investigated. These optimization questions will be the focus of the present study.

Motivated by gastropod locomotion (e.g. Vlès 1907; Denny 1980) and recent studies of self-propelled liquid-crystal elastomers (Camacho-Lopez *et al.* 2004), we consider a variation on Taylor's swimming sheet, namely a flexible membrane swimming on top of a viscous fluid (see Figure 1). In this geometry the membrane sits at a free surface and fluid is present on only one side of the sheet. This configuration is similar to that adopted by crawling gastropods that propel themselves via an unusual mechanism known as adhesive locomotion. As a snail or slug crawls, the organism secretes a thin film of fluid between the flexible foot and the substrate (Figure 1a). The animal propels itself by generating waves along the bottom of the foot which in turn generate stresses within the thin film. In real snails, the rheological properties of this film are highly nonlinear; however, we will begin by considering the simplest case of a periodically deforming membrane on top of a Newtonian fluid†.

The second phenomenon that motivated the current study is the recently observed "swimming" motion of liquid-crystal elastomers (LCEs). When a small LCE disk at an air/water interface is triggered with a laser, the elastomer will "swim into the dark" by generating a wave along the flexible body. Again, the geometrical configuration is similar to that shown in Figure 1. In both of these examples, we are particularly interested in organisms that swim or crawl on a thin film of fluid near a rigid boundary. It has been well-documented that the presence of such a boundary can dramatically affect the behaviour of low Reynold number swimmers; e.g. bacteria swimming near a rigid boundary tend to swim in circles (rather that in a random walk) due to hydrodynamic interactions with the wall (Lauga *et al.* 2006; DiLuzio *et al.* 2005). It has been argued that the interaction of rigid boundaries with low Reynolds number propulsion systems, may be relevant to the early stages of biofilm formation and of pathogenic infection (DiLuzio *et al.* 2005).

In the current study we will consider "optimal" geometries for low Reynolds number swimmers near a rigid boundary. In section 2 we define the mathematical model, calculate swimming velocities in the lubrication limit, and compare the accuracy of the full Stokes' flow solution to the lubrication results. In section 3, we define three optimization questions and formulate the relevant Euler-Lagrange equations. In section 4, we present two numerical methods to solve the optimization problems posed in section 3, and end with a brief discussion in section 5.

2. Mathematical Model

Our swimming "organism" can be roughly modeled as a flexible sheet waving in a viscous fluid near a rigid boundary. In the simplest case, we can assume that the foot shape is periodic and completely determined by the muscular input; thus we assume that the snail can select a foot deformation that is most effective for a given environment. Consider a one dimensional sheet swimming over a two dimensional Stokesian fluid as shown in Figure 1(b). The wave profile and the fluid velocity are assumed to be periodic in the x-direction with period W. The fluid is bounded on the bottom by a flat wall which is stationary in the lab frame. The system is assumed to have reached its steady state so that there is a reference frame (the wave frame) in which the wave envelope

---

† While this model is not ideal for real gastropods, it is directly relevant to the design of mechanical crawlers in which the mucus simulant may be chosen to be Newtonian (Chan *et al.* 2005).
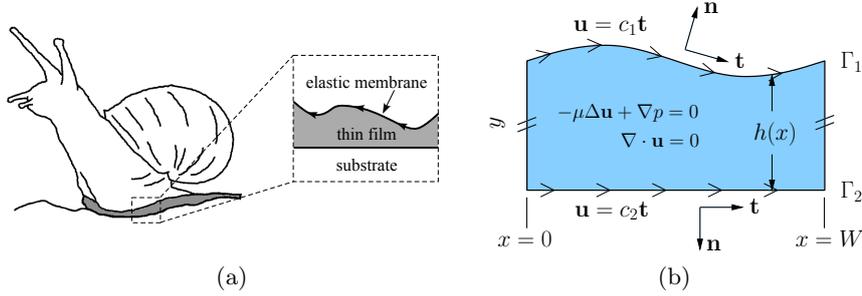
FIGURE 1. (a) Schematic of gastropod locomotion showing a thin viscous fluid sandwiched between a periodically deforming flexible foot and a rigid substrate. (b) Idealized model depicting steady state swimming of a sheet via wave propagation. This system is conveniently studied in the reference frame in which the wave profile Γ_1 remains stationary. In this frame, material points on the sheet move tangent to Γ_1 with constant speed c_1 and the wall moves with contant speed c_2.

$\Gamma_1 = \{(x, h(x))\}$ (i.e. the shape of the foot) remains stationary in time. In this frame, the wall moves with constant velocity c_2 in the x-direction while the sheet moves tangent to Γ_1 with constant speed c_1; thus, the sheet remains inextensible as it swims. Our goal is to study the effect of the curve shape on the swimming speed and the power required to swim, and to find optimal shapes that maximize speed or efficiency subject to given constraints (e.g. holding fixed the membrane length $L = \int_0^W \sqrt{1 + h'(x)^2}\, dx$ and fluid volume $A = \int_0^W h(x)\, dx$, where $h(x)$ is the local film thickness and subscripts denote partial derivatives). Since the optimal shapes turn out not to exhibit infinite slopes or singularities, it does not appear necessary to pose the problem more generally to allow the wave profile to overturn.

2.1. *Swimming Speed and Power Dissipation*

In the following sections, we will restrict our analysis to the long wavelength limit. However, before we consider this limit, it is useful to derive certain quantities and constraints that are generally true for Stokes flow, independent of geometry. If $c_1, c_2 \in \mathbb{R}$ and $h(x)$ is a sufficiently smooth periodic function, there is a unique solution to the Stokes' equations

$$\nabla p = \mu \nabla^2 \mathbf{u} \qquad \nabla \cdot \mathbf{u} = 0 \tag{2.1}$$

subject to the boundary conditions shown in Figure 1. Here p denotes pressure, μ is the dynamic viscosity and $\mathbf{u}$ is the velocity field within the thin film. Given this solution, we can calculate the relevant forces and powers required for steady state swimming in terms of the stress tensor $\sigma = (\nabla \mathbf{u} + \nabla \mathbf{u}^T)$, namely

$$P(c_1, c_2) = \int_{\Gamma_1} \mathbf{t} \cdot \sigma \mathbf{n}\, ds, \qquad F(c_1, c_2) = -\int_{\Gamma_1} \mathbf{e}_1 \cdot \sigma \mathbf{n}\, ds = \int_{\Gamma_2} \mathbf{t} \cdot \sigma \mathbf{n}\, ds \tag{2.2}$$

where $\mathbf{e}_1$ is the unit vector in the direction of motion and $\mathbf{t}$ and $\mathbf{n}$ denote respectively unit tangent and normal vectors to the membrane/fluid interface. Physically, $c_1 P$ is the power required to maintain the steady motion of the sheet, F is the x-component of the net force exerted by the fluid on the sheet (which is the same as that exerted by the bottom wall on the fluid), and $c_2 F$ is the power required to maintain the steady motion of the bottom wall (in the wave frame). Assuming the forces exerted by the sheet on the fluid are internally generated (e.g. by the muscles in the snail or by an internal motor in a mechanical crawler), we require $F = 0$ in steady state. Since the Stokes equations are

linear, $F(c_1, c_2) = c_1 F(1, 0) + c_2 F(0, 1)$ and we obtain the relationship

$$c_2 = -\frac{F_1}{F_2} c_1, \qquad (2.3)$$

where $F_1 = F(1, 0)$ and $F_2 = F(0, 1)$. We note that c_1 is directly controlled by the swimmer: $(W/L)c_1$ is the speed at which the sheet propagates waves to the left (relative to its material points) in order to swim to the right. Hence, the swimming speed in the lab frame is given by

$$c = \frac{W}{L} c_1 - c_2 = \left(\frac{W}{L} + \frac{F_1}{F_2} \right) c_1. \qquad (2.4)$$

It is useful to derive expressions for P and F in terms of the velocity field $\mathbf{u} = (u, v)$. To this end, we substitute $ds|_{\Gamma_1} = \sqrt{1 + h_x^2}\, dx$ and a Newtonian stress tensor,

$$\sigma = -pI + \mu \begin{pmatrix} 2u_x & u_y + v_x \\ u_y + v_x & 2v_y \end{pmatrix}, \quad \mathbf{t}|_{\Gamma_1} = \frac{(1, h_x)}{\sqrt{1 + h_x^2}}, \quad \mathbf{n}|_{\Gamma_1} = \frac{(-h_x, 1)}{\sqrt{1 + h_x^2}} \qquad (2.5)$$

into (2.2) and use continuity 2.1 to obtain

$$P(c_1, c_2) = \int_{\Gamma_1} \mu \frac{-4u_x h_x + (u_y + v_x)(1 - h_x^2)}{\sqrt{1 + h_x^2}}\, dx, \qquad (2.6)$$

$$F(c_1, c_2) = \int_{\Gamma_1} -p h_x + \mu \left[2u_x h_x - (u_y + v_x) \right] dx = \int_{\Gamma_2} -\mu(u_y + v_x)\, dx. \qquad (2.7)$$

Here x and y subscripts denote partial derivatives. We then use the boundary conditions $u(x, h(x)) = c_1(1 + h_x^2)^{-1/2}$ and $v(x, h(x)) = c_1 h_x(1 + h_x^2)^{-1/2}$ (no slip at, and no flux through the membrane) to conclude that, on Γ_1, $u_x = -(u_y + \kappa c_1)h_x$ and $v_x = \kappa c_1 - v_y h_x = \kappa c_1 + u_x h_x = \kappa c_1(1 - h_x^2) - u_y h_x^2$, where $\kappa = h_{xx}(1 + h_x^2)^{-3/2}$ is the curvature of the interface. Substituting these into (2.6) and (2.7) gives $P(c_1, c_2) = \int_{\Gamma_1} \mu(u_y + \kappa c_1)(1 + h_x^2)^{3/2}\, dx$ and $F(c_1, c_2) = \int_{\Gamma_1} -p h_x - \mu(u_y + \kappa c_1)(1 + h_x^2)\, dx = \int_{\Gamma_2} -\mu u_y\, dx$. The terms involving κ are derivatives of periodic functions and vanish when integrated, thus

$$P(c_1, c_2) = \int_{\Gamma_1} \mu u_y (1 + h_x^2)^{3/2}\, dx, \qquad (2.8)$$

$$F(c_1, c_2) = \int_{\Gamma_1} -p h_x - \mu u_y (1 + h_x^2)\, dx = \int_{\Gamma_2} -\mu u_y\, dx. \qquad (2.9)$$

We note that because $F_2 = F(0, 1)$ is numerically equal to the power required to maintain a unit speed of the bottom wall while holding the top sheet fixed, it is necessarily positive. Likewise, the power $P(1, 0)$ required to push the top sheet along the curve $h(x)$ while holding the bottom wall fixed is also positive. One might expect that the x-component of the net force $-F(1, 0)$ applied during this process would also be positive. Surprisingly, this turns out not to be true. The pressure term in (2.9) can dominate the viscous drag term so that $F_1 > 0$, $c_2 < 0$ and $c > c_1$, i.e. the organism can move *faster* than the wave speed. This was first observed in the lubrication limit by Chan *et al.* (2005) in their study of snail locomotion.

2.2. *The Lubrication Approximation*

We now briefly review the work of Chan *et al.* (2005) in which the authors compute the swimming speed of the sheet in the lubrication (i.e. small amplitude) limit (Reynolds 1886). To study the small amplitude limit, $h \ll W$, we non-dimensionalize the problem, choosing different scales for the x- and y-coordinates to keep the rescaled aspect ratio of

the domain of order unity. Specifically, we choose a characteristic height H (e.g. average gap thickness) and velocity V (e.g. wave speed) and set $\hat{x} = Wx$, $\hat{y} = Hy$, $\hat{h}(\hat{x}) = Hh(x)$, $\hat{c}_i = Vc_i$, $\hat{\mathbf{u}} = V\mathbf{u}$, and $\hat{p} = \frac{\mu VW}{H^2}p$, where, hence forward, the carat distinguishes a physical variable from its dimensionless counterpart. (Note that in the previous section, all variables are dimensional variables). Dropping terms of order H/W, the momentum equations (2.1) become $p_x = u_{yy}$ and $p_y = 0$. To first order in H/W, the boundary conditions on u are $u(x, h(x)) = c_1$, $u(x, 0) = c_2$; hence, the fluid velocity is given by

$$u(x, y) = \frac{y}{2}(y - h)p_x + \frac{y}{h}c_1 + \left(1 - \frac{y}{h}\right)c_2. \tag{2.10}$$

Integrating from 0 to h and solving for p_x, we obtain

$$p_x = \frac{6}{h^2}(c_1 + c_2) - \frac{12}{h^3}Q, \tag{2.11}$$

where $Q = \int_0^h u\,dy = $ constant is the volume flux through any cross section of the fluid. Since p_x is periodic, $\int_0^1 p_x\,dx = 0$ and we find that

$$Q = \frac{c_1 + c_2}{2}\frac{I_2}{I_3}, \qquad \text{where} \qquad I_k = \int_0^1 h(x)^{-k}\,dx. \tag{2.12}$$

The terms involving h_x in (2.8) and (2.9) vanish in the lubrication limit. Explicitly, if we set $\hat{P} = \mu V\frac{W}{H}P$, $\hat{F} = \mu V\frac{W}{H}F$ and drop lower order terms, we obtain

$$P = \int_{\Gamma_1} u_y\,dx, \qquad F = \int_{\Gamma_1} p_x h - u_y\,dx = \int_{\Gamma_2} -u_y\,dx. \tag{2.13}$$

Substituting $u_y = 6(c_1 + c_2)(y - h/2)(1/h^2 - I_2/(I_3 h^3)) + (c_1 - c_2)/h$ from above and integrating, we obtain power and force functions in the lubrication limit

$$P = \left(4I_1 - 3\frac{I_2^2}{I_3}\right)c_1 + \left(2I_1 - 3\frac{I_2^2}{I_3}\right)c_2 \tag{2.14}$$

$$F = \left(2I_1 - 3\frac{I_2^2}{I_3}\right)c_1 + \left(4I_1 - 3\frac{I_2^2}{I_3}\right)c_2. \tag{2.15}$$

It follows from (2.3) and (2.4) that

$$c_2 = -\frac{2 - 3\zeta}{4 - 3\zeta}c_1, \qquad c = \frac{6(1 - \zeta)}{4 - 3\zeta}c_1 \tag{2.16}$$

where the shape parameter, ζ, is defined as

$$\zeta = \frac{I_2^2}{I_1 I_3}. \tag{2.17}$$

Finally, we use (2.16) and (2.14) to obtain the power that must be generated by the sheet in order to swim at steady state:

$$\text{power} = c_1 P = 2I_1 c_1 c. \tag{2.18}$$

A natural choice for the characteristic speed V is the wave speed, in which case $c_1 = 1$. We remark that the Cauchy-Schwartz inequality gives

$$I_2^2 = \left(\int h^{-1/2} h^{-3/2}\,dx\right)^2 \leq \int h^{-1}\,dx \int h^{-3}\,dx = I_1 I_3, \tag{2.19}$$

hence $0 < \zeta \leq 1$ and $0 \leq c < 3/2$. There are many families of curves for which the swimming speed c approaches its maximal value of $3/2$. Generally speaking, this requires
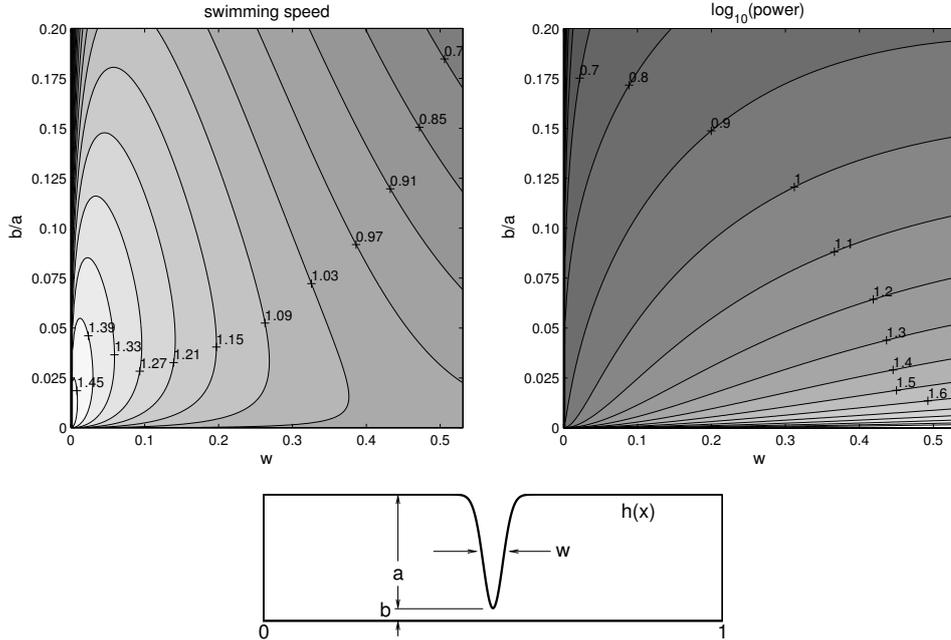
FIGURE 2. Contour plots of swimming speed c and power P as functions of gap thickness b and ripple width w for the wave profile $h(x) = b + a[1 - (\sin^2(\pi x))^{\frac{4\log 2}{\pi^2 w^2}}]$. If $w > 0$ is held fixed, $c \to 1$ and $P \to \infty$ as $b \to 0$. If $b > 0$ is held fixed, $c \to 0$ and $P \to 0$ as $w \to 0$. If the ratio b/w is held fixed, $c \to 3/2$ and P remains bounded as $b, w \to 0$.

that, locally, the wave profile nearly touches the wall and becomes sharp as it does so (see Figure 2). Physically, when the wave profile has a minimum close to the wall, a large pressure jump across the constricted fluid gap develops which pushes the sheet forward against the viscous drag forces. Hence, we expect the fastest profiles to be those that: (1) nearly touch down (so the pressure jump is large); (2) have wave profiles that are nearly vertical in the neighborhood of the touchdown (so the pressures act on surfaces that are oriented perpendicular to the direction of motion); and (3) the touchdown region is small to minimize drag. However, in the limit as the gap thickness approaches zero, if the curvature of the profile at the touchdown point remains finite, it is not difficult to show (Chan *et al.* 2005) that the shape parameter ζ will approach $2/3$ and the speed c will approach 1. Therefore, to achieve speeds greater than the wave speed, the curvature must become singular as the gap thickness goes to zero in order to approach the maximal speed $c = 3/2$. For the family of wave profiles shown in Figure 2, the curvature κ at the minimum is given by $\kappa = \frac{8a\log 2}{w^2}$. One may show that, as $b \to 0$, holding b/w fixed, the speed approaches $3/2$ and the power remains bounded; however, it is worth remembering that the lubrication approximation eventually breaks down when the ripple becomes too sharp.

2.3. *Validity and Limitations of the Lubrication Approximation*

In this section we compare the swimming speed and power predicted by the lubrication approximation to a finite element computation of the full Stokes' equations for a family of test cases. This validation in particularly important in our case as the most interesting profiles, namely those that become sharp near touchdown, are precisely those in which we expect the lubrication approximation to fail. Hence limits on the validity of lubrication in

these geometries need to be established. The lubrication approximation gives the zeroth order terms in an expansion of the solution in powers of $\varepsilon = H/W$. In Appendix A, we derive formulas for the second and fourth order terms in this expansion as well; the terms with odd powers of ε are zero. Taking $c_1 = 1$ and writing

$$c = c^{(0)} + \varepsilon^2 c^{(2)} + \varepsilon^4 c^{(4)} + \cdots, \qquad P = P^{(0)} + \varepsilon^2 P^{(2)} + \varepsilon^4 P^{(4)} + \cdots, \qquad (2.20)$$

we obtain

$$c^{(0)} = \frac{6(1-\zeta)}{4-3\zeta}, \qquad (2.21)$$

$$c^{(2)} = \frac{1}{10(4-3\zeta)^2} \left[(8+10\zeta)\frac{E_1}{I_1} + 48\zeta\frac{E_3}{I_3} - (44\zeta + 15\zeta^2)\frac{E_2}{I_2} \right] - \frac{E_0}{2I_0}, \qquad (2.22)$$

$$P^{(0)} = 2I_1 c, \qquad (2.23)$$

$$P^{(2)} = \frac{6I_1}{5(4-3\zeta)^2} \left[(8-10\zeta+5\zeta^2)\frac{E_1}{I_1} - (4\zeta+5\zeta^2)\frac{E_2}{I_2} + 8\zeta\frac{E_3}{I_3} \right], \qquad (2.24)$$

with similar expressions for $c^{(4)}$ and $P^{(4)}$ where superscript numbers in parentheses indicate the order of the expansion; see (A 23)–(A 26) and (A 31)–(A 33) for details. Here

$$E_k \equiv \int_0^1 \frac{h_x^2}{h^k} \, dx. \qquad (2.25)$$

Note that the terms E_k/I_k are weighted averages of h_x^2 with weight function h^{-k}. The formulas for $c^{(4)}$ and $P^{(4)}$ also involve ζ and various weighted averages of the form E_k/I_k, J_k/I_k, G_k/I_k, $(k = 0, 1, 2, 3)$, where $J_k = \int_0^1 \frac{h_x^4}{h^k} \, dx$ and $G_k = \int_0^1 \frac{h^2 h_{xx}^2}{h^k} \, dx$ (see Appendix A).

To study the range of validity of these formulas, we compare them to finite element calculations of the full Stokes' equations for a family of test cases. The wave profiles considered are of the form

$$\hat{h}(x) = Hh(x), \qquad h(x) = b + a[1 - (\sin^2 \pi x)^k], \qquad (a = t, \ b = 1 - t). \qquad (2.26)$$

Here H varies between 0.015 and 0.15, t varies between 0 and 1, and $k = 10$ is held fixed. Note that when $t = 0$, $h(x) \equiv 1$ and when $t \to 1$, $h(x)$ touches down with a locally parabolic profile. In the finite element calculations, we use a logically rectangular grid with nodes $\mathbf{x}_{ij} = (x_i, \hat{h}(x_i)j/N)$, $0 \le i \le M$, $0 \le j \le N$ (see Figure 3). The mesh is triangulated by cutting quadrilaterals along their shortest diagonal. The x_i are spaced to keep the aspect ratios of the triangles as close to 1 as possible, which requires $x_{i+1} - x_i \approx \hat{h}(x_i)/N$. This is easily done by choosing M to be the nearest integer to $N\hat{I}_1 = N \int_0^1 \hat{h}(x)^{-1} \, dx$, solving the ODE $x'(s) = \hat{I}_1\hat{h}(x(s))$, and setting $x_i = x(i/M)$. We used a variant of the First Order System Least Squares finite element method (Cai *et al.* 1997) to solve the Stokes' equations (2.1) using quadratic elements (with curved boundaries on the top wall) for all six variables $w = (u, v, p, \omega, \gamma, \tau)$; here ω is the vorticity, and γ and τ are shear stresses. We solved the equations using a multigrid preconditioned conjugate gradient method; this method is extremely fast, i.e. the equations can be solved in a few minutes for problem sizes all the way up to the point where we run out of computer memory (8 GB) storing the variables and multigrid data structures. For each geometry, we solve the Stokes equations twice: once with boundary conditions $c_1 = 1$, $c_2 = 0$, and once with boundary conditions $c_1 = 0$, $c_2 = 1$. Using formulas (2.8) and (2.9), these computations give $F(1,0)$, $P(1,0)$, $F(0,1)$, $P(0,1)$, which are sufficient to
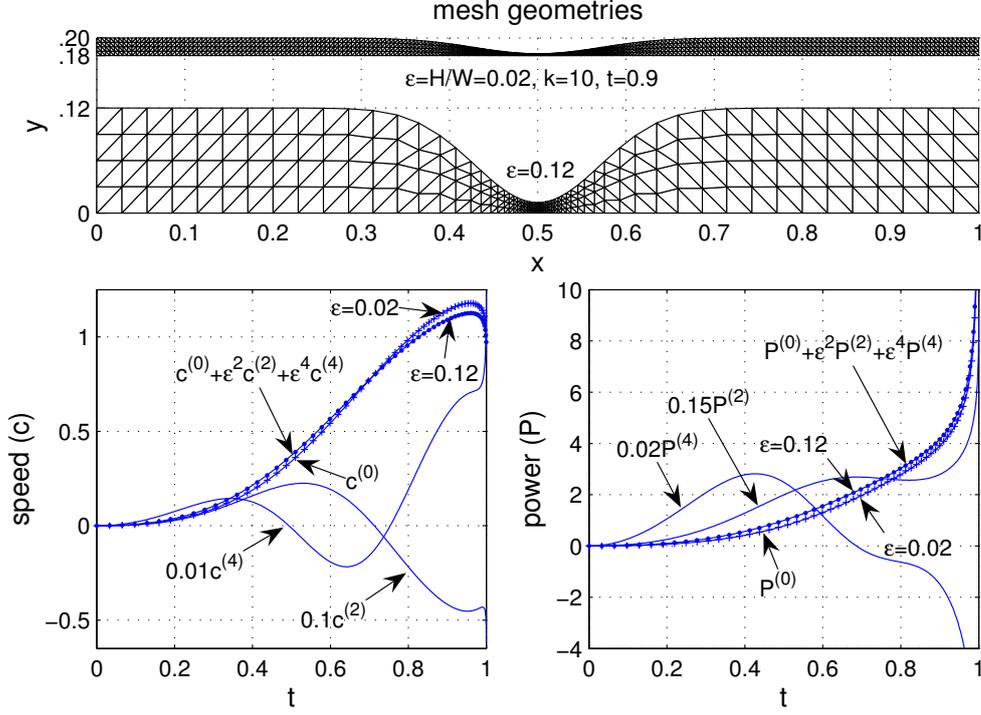
FIGURE 3. Top: two of the mesh geometries (coarsened for visibility) used to compute the dependence of speed and power on t and H. Bottom: comparison of the finite element results (denoted by dots) with the lubrication theory (solid curve under the $\varepsilon = 0.02$ results) and the 4th order, $\varepsilon = 0.12$ correction. Note, the zeroth order solution has no dependence on ε. Hence the solid line (under $\varepsilon = 0.02$) represents the zeroth order approximation for both the $\varepsilon = 0.02$ and the $\varepsilon = 0.12$ cases. Also shown are the expansion coefficients used to compute the 4th order correction.

compute the swimming speed and power

$$c = \frac{W}{L} + \frac{F(1,0)}{F(0,1)}, \qquad \text{power} = P(1,0) - \frac{F(1,0)}{F(0,1)}P(0,1). \qquad (2.27)$$

We normalize these solutions by multiplying the power by H/μ. Recall that the actual power is related to the non-dimensionalized power via $\hat{c}_1\hat{P} = \mu V^2 \frac{W}{H}c_1 P$; the finite element solutions have already been partially non-dimensionalized by setting $V = 1$, $c_1 = 1$, $W = 1$.

In Figure 3, we show the results of two sequences of finite element computations in which t varies from 0 to 1, one with $H = 0.02$ and one with $H = 0.12$. The meshes at the top have parameters $t = 0.9$, $N = 4$, $M_{0.02} = 344$, $M_{0.12} = 60$. The computations at the bottom were performed with $N = 48$; to maintain proper spacing in the x-direction, $M_{0.02}$ ranged from 2400 ($t = 0$) to 13152 ($t = 0.996$) while $M_{0.12}$ ranged from 432 ($t = 0$) to 7920 ($t = 0.99972$). The $H = 0.02$ computation agrees nicely with the lubrication prediction (shown with a solid line) even for parameter ranges in which the crawling speed exceeds the wave speed. The $H = 0.12$ computation deviates visibly from the lubrication prediction, but agrees well with the 4th order correction, which is also shown with a solid line. Note that the zeroth order solution does not depend on ϵ and hence
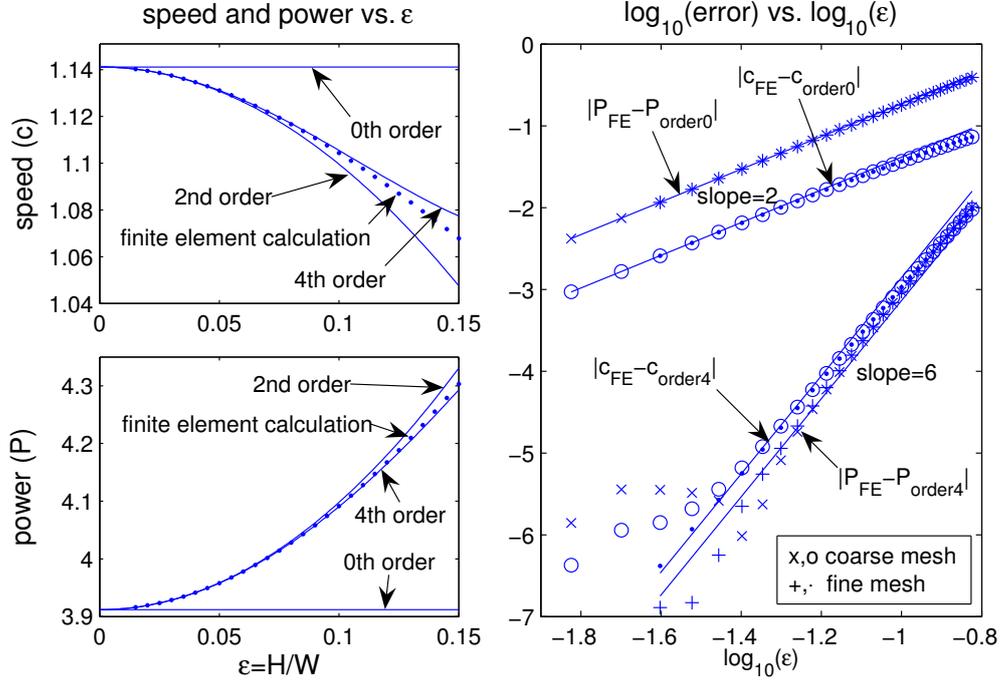
FIGURE 4. Comparison of the lubrication theory and its corrections to the finite element results as H ranges from 0.015 to 0.15 with $t = 0.9$ held fixed.

predicts the same velocities for both the $H = 0.02$ and the $H = 0.12$ case. The final two curves in each graph show the coefficients $c^{(2)}$, $c^{(4)}$, $P^{(2)}$, $P^{(4)}$ used to compute the 4th order correction, using formulas (A 24), (A 25), (A 32), and (A 33). In Figure 4, we hold $t = 0.9$ fixed and vary H from 0.015 to 0.15 using $N = 64$, $M_{0.015} = 7360$, $M_{0.15} = 768$. We also used a finer mesh, letting H vary from 0.025 to 0.15 with $N = 96$, $M_{0.025} = 6624$, $M_{0.15} = 1152$. As expected, we see that the error term associated with using the zeroth order lubrication theory is $O(\varepsilon^2)$; using the second and 4th order corrections to the lubrication theory lead to errors which are $O(\varepsilon^4)$ and $O(\varepsilon^6)$, respectively. Numerical error in the finite element computation is responsibly for the scatter in the computed error of the 4th order correction when ε is small; in this regime, it is clearly more accurate to use the expansion solutions instead of finite elements.

It is quite remarkable that the lubrication theory works so well as the geometries we tested against the finite element simulations deviate substantially from the flat profiles envisioned in the derivation of the theory. This can be roughly explained by arguing that the largest boost from the pressure gradient occurs in the vicinity of the touchdown which is precisely where we expect lubrication to do well; the details of the outer flow where lubrication fails, are unimportant in calculating crawling velocities. Therefore, it seems worthwhile to study the shape optimization problem within the context of lubrication theory and check the sizes of the correction terms $c_2^{(k)}$, $P^{(k)}$ afterwards to determine how small $\varepsilon = H/W$ must be chosen for the results to be valid. It is noteworthy that the correction terms may be expressed in terms of weighted averages (E_k/I_k, J_k/I_k, etc.) of the slopes and higher derivatives of h with respect to inverse powers of h. This gives

us some intuition about the features of a solution which affect its validity beyond the lubrication approximation, i.e. if E_k/I_k is small for $k = 1, 2, 3 \ldots$ then $c_2^{(}2)$ and $P^{(}2)$ are also small. Thus the validity of the lubrication approximation is determined by the magnitude of h_x^2 is near touchdown, where h is small.

3. Optimization: Euler-Lagrange Equations

In this section we describe three natural optimization problems in the context of swimming sheets namely, for a sheet of fixed length swimming on top of a fixed volume of fluid:
- (*a*) Maximize the swimming speed
- (*b*) Maximize the efficiency
- (*c*) Maximize the efficiency for a given swimming velocity.

We work out the associated Euler-Lagrange equations for each of these optimization questions in the lubrication limit. Although this approximation is zeroth order, the arclength $\hat{L} = \int_0^W (1 + \hat{h}_{\hat{x}}^2)^{1/2} \, d\hat{x}$ must be treated at second order to obtain zeroth order results for swimming speed and power. Therefore, we expand $\hat{L} \approx W \left(1 + \frac{H^2}{W^2} \ell^2\right)$ and drop higher order terms, where $\ell^2 = \frac{1}{2} \int_0^1 h_x^2 \, dx$. A scaling argument (presented below) provides further justification. In all of these cases we will consider a given $\ell_0 > 0$ and $A_0 > 0$ defined by

$$\ell_0 \equiv \frac{1}{2} \int_0^1 h_x^2 \, dx, \qquad A_0 \equiv \int_0^1 h \, dx. \tag{3.1}$$

Problem 1 (maximize speed). In the first case, we wish to find the function $h(x)$ that maximizes the speed c in (2.16) subject to the constraints (3.1) given above . Since $c(\zeta) = \frac{6(1-\zeta)}{4-3\zeta}$ is a monotonically decreasing function of ζ on the unit interval, this problem is equivalent to minimizing $\zeta = \frac{I_2^2}{I_1 I_3}$. For a general functional $f[h]$, let us denote its first variation by a prime (when it exists) so that

$$Df[h]g \equiv \int_0^1 f'[h](x)g(x) \, dx. \tag{3.2}$$

In particular,

$$I_k' = -kh^{-k-1}, \quad \zeta' = \left(\frac{1}{I_1 h^2} - \frac{4}{I_2 h^3} + \frac{3}{I_3 h^4}\right)\zeta, \quad (\ell^2)' = -h_{xx}, \quad A' = 1. \tag{3.3}$$

Assuming an optimal solution exists which is at least C^2, it must satisfy the equation $\zeta' + \lambda_1 (\ell^2)' + \lambda_2 A' = 0$ for some Lagrange multipliers, λ_1, λ_2. For this problem, it is possible to compute these Lagrange multipliers analytically. To this end, consider the new objective function

$$F[h] = \zeta[\alpha h + \beta] + (\alpha - 1)^2/2 + \beta^2/2, \tag{3.4}$$

where $\alpha = \ell_0(\frac{1}{2} \int h_x^2 \, dx)^{-1/2}$ and $\beta = A_0 - \alpha \int h \, dx$ are chosen so that $\alpha h + \beta$ satisfies the constraints. Any global minimizer of F will be a constrained minimizer of ζ and satisfy $\alpha = 1$, $\beta = 0$. Note that

$$\frac{d}{d\varepsilon}F[h + \varepsilon g] = \int \zeta'[\alpha h + \beta] \left[\alpha g + h \int \alpha' g \, dx + \int \beta' g \, dx\right] + (\alpha - 1)\alpha' g + \beta\beta' g \, dx,$$

hence

$$F'[h] = \alpha\zeta' + \left(\int \zeta' h\, dx\right)\alpha' + \left(\int \zeta'\, dx\right)\beta' + (\alpha - 1)\alpha' + \beta\beta', \qquad (3.5)$$

where ζ' is evaluated at $\alpha h + \beta$ in each of the integrals. One readily checks that $\alpha' = \frac{\alpha^3}{2\ell_0^2}h_{xx}$ and $\beta' = -\int h\, dx\, \alpha' - \alpha$. Setting $\alpha = 1$, $\beta = 0$, $F'[h] = 0$ we obtain $\zeta' - \left(\int \zeta'\, dx\right)\left(\frac{A_0}{2\ell_0^2}h_{xx} + 1\right) = 0$, which leads to the integro-differential equation,

$$h_{xx} = \left(\frac{2\ell_0^2}{A_0}\right)\left(\frac{h^{-2}/I_1 - 4h^{-3}/I_2 + 3h^{-4}/I_3}{I_2/I_1 - 4I_3/I_2 + 3I_4/I_3} - 1\right). \qquad (3.6)$$

In Section 4 we will present a robust numerical method based on (3.4) and (3.5) for to find solutions to this problem. We will also present a fast, highly accurate method of solving the IDE (3.6) once an initial guess is known for each I_k and $h(0)$.

Although there are two parameters (ℓ_0 and A_0) in the problem statement, if we scale both by the same factor θ, the optimal solution h merely scales by θ as well, and the optimal speed remains the same. This is clear from the Euler-Lagrange equation (3.6) and the formula $\zeta = I_2^2/(I_1 I_3)$, noting that when $h \to \theta h$, $I_k \to \theta^{-k} I_k$. This is to be expected from the formulation in the lubrication limit since the analysis is intended to hold independently of the small parameter H/W, and the physical problem remains unchanged if we replace h by θh and H by $\theta^{-1}H$. Therefore, there is only a one relevant parameter and we seek a family of optimal solutions depending on the ratio A_0/ℓ_0.

This problem becomes singular as the (dimensionless) area becomes small relative to the linearized arclength as the curve touches down. Consider the extreme limit in which the curve has touched down. Choosing the location of touchdown to be at the edges of our periodic interval, $h(0) = h(1) = 0$, and $\frac{1}{2}\int_0^1 h_x^2\, dx = \ell_0^2$; then, the maximal area under h is achieved by the function $h(x) = \sqrt{6}\ell_0(x - x^2)$, which has (dimensionless) area $A_{\text{crit}} = \ell_0/\sqrt{6}$. Therefore, if $A_0 > A_{\text{crit}}$, any periodic function $h(x)$ which satisfies the constraints (3.1) is strictly positive. In Section 4.2 we will study the asymptotics of the solution as A_0 approaches this critical value. They appear to be self-similar in the neighborhood of the touchdown point and approach the parabola $h(x) = \sqrt{6}\ell_0(x - x^2)$ elsewhere, where the complicated term involving I_k's on the RHS in (3.6) becomes negligible. They also approach the optimal speed $c = 1.5$, but require an infinite amount of power in this limit.

Problem 2 (maximize efficiency). In this second case, we wish to find the shape function h which maximizes the ratio of speed to power (i.e. the "efficiency") subject to the constraints (3.1). From (2.18), we see that $c/P = 1/(2I_1)$, thus to maximize this ratio, we must minimize I_1. Taking the same approach as before, we set

$$F[h] = I_1[\alpha h + \beta] + (\alpha - 1)^2/2 + \beta^2/2 \qquad (3.7)$$

and compute

$$F'[h] = \alpha I_1' + \left(\int I_1' h\, dx\right)\alpha' + \left(\int I_1'\, dx\right)\beta' + (\alpha - 1)\alpha' + \beta\beta', \qquad (3.8)$$

where I_1' is evaluated at $\alpha h + \beta$ in each of the integrals. Setting $\alpha = 1$, $\beta = 0$, $F'[h] = 0$ we obtain $I_1' - I_1\alpha' + I_2(A_0\alpha' + 1) = 0$, i.e.

$$h_{xx} = 2\ell_0^2 \frac{h^{-2} - I_2}{I_2 A_0 - I_1}. \qquad (3.9)$$

Interestingly, in Section 4 we will see that solutions to this equation maximize I_1 rather than minimize it. There are well behaved functions h which are optimally *inefficient, but

one cannot achieve the optimal efficiency $c/P = A_0/2$. Moreover, in order to approach this efficiency, the swimming speed must go to zero; therefore, it seems more useful to reformulate the problem as follows.

Problem 3 (maximize efficiency for a given swimming speed). Given an attainable speed c, we wish to find the shape function h which minimizes the power required to swim at this speed. Because the speed constraint is non-trivial, we cannot obtain analytic expressions for the Lagrange multipliers, and must be satisfied leaving the Euler-Lagrange equation $P' + \lambda_1(\ell^2)' + \lambda_2 c' + \lambda_3 A' = 0$ in the form

$$h_{xx} = -\frac{\lambda_1}{h^2} - \frac{4\lambda_2}{I_2 h^3} + \frac{3\lambda_2}{I_3 h^4} + \lambda_3, \qquad (3.10)$$

where we have used $c' = \frac{-6}{(4-3\zeta)^2}\zeta'$, $P' = 2(I_1'c + I_1 c')$, and redefined the Lagrange multipliers to simplify the equation.

4. Numerical Methods and Results

In this section we describe two numerical methods for solving the optimization problems posed in the previous section and analyze the results. In the first approach, we represent the shape function h using periodic cubic splines and use a limited memory BFGS method (Nocedal & Wright 1999) to descend to the optimal shape. In the second approach, we solve the Euler-Lagrange equations using a quadratically convergent Levenberg-Marquardt method to vary the parameters of the ODE until the constraints are satisfied. The first approach is fast and robust unless the solution is very singular. It also gives useful information in cases where the optimization problem has no solution. The second approach requires a good starting guess, but is otherwise fast and highly accurate even when the solution is nearly singular.

We use the first approach to study Problems 1 and 2 of the previous section, but not Problem 3 — the additional velocity constraint requires a significant modification of the algorithm. We use the second approach to study Problems 1 and 3; it can be used for Problem 2 as well, however, as the solution minimizes efficiency instead of maximizing it, the result is less interesting and we omit the details. Finally, we compute the second and fourth order corrections to the lubrication theory to conclude that the lubrication approximation remains uniformly valid for Problem 1 even in the critical limit $A_0 \to \ell_0/\sqrt{6}$, but breaks down for Problem 3 in the critical limit $\zeta_0 \to 0$ due to the formation of a cusp in the optimal shape.

4.1. *Direct Minimization using Periodic Cubic Splines*

Problem 1 (maximize speed). The basic strategy in this section is to represent the function h using periodic cubic splines (Carl de Boor 2001) and use a gradient-based minimization algorithm (limited memory BFGS (Nocedal & Wright 1999)) to modify the degrees of freedom in the spline space in order to minimize the functional $F[h]$ in (3.4). We start with relatively few knots in the spline space (typically 32 or 64) and find the optimal shape in this space. We then repeatedly double the number of knots using the previous solution as the starting guess until the variational derivative $F'[h]$ is sufficiently small.

The key to this algorithm is finding an efficient way to compute the gradient of the discretized system. Let us denote the spline basis functions by φ_i. Each φ_i is a periodic piecewise cubic C^2 function satisfying $\varphi_i(x_j) = \delta_{ij}$ at the knots x_j. Each $q \in \mathbb{R}^n$ is associated with a unique spline function $h_q(x) = \sum_{i=1}^{n} q_i \varphi_i(x)$, which satisfies $h_q(x_i) =$

q_i. Our goal is to minimize the function

$$f(q) = F[h_q], \qquad (4.1)$$

where $F[h]$ was given in (3.4). The gradient $g = \nabla f$ is given by

$$g_i = \int F'[h_q]\frac{\partial h_q}{\partial q_i}\, dx = \int F'[h_q]\varphi_i\, dx. \qquad (4.2)$$

Because the φ_i are supported on the entire unit interval, it is more efficient to compute g using B-splines, which have compact support. We use standard spline formulas (Carl de Boor 2001) to find the coefficients a_i, b_i, c_i to express $B_i(x) = a_i\varphi_{i-1}(x) + b_i\varphi_i(x) + c_i\varphi_{i+1}(x)$, taking care to wrap around the endpoints of the unit interval as necessary to handle periodicity. Instead of computing g_i in (4.2) directly, we first compute

$$\tilde{g}_i = \int F'[h_q]B_i\, dx = a_i g_{i-1} + b_i g_i + c_i g_{i+1} \qquad (4.3)$$

by integrating against the compactly supported B-splines, and then solve the equation $Tg = \tilde{g}$, where T is almost tridiagonal: $T_{i,i-1} = a_i$, $T_{ii} = b_i$, $T_{i,i+1} = c_i$; except for the two entries that fall out of bounds and are wrapped around: $T_{1n} = a_1$, $T_{n1} = c_n$. This reduces the cost of computing g from $O(n^2)$ to $O(n)$. To compute $F'[h_q]$ in (4.3), we simply evaluate the formulas

$$\alpha[h] = \ell_0 \left(\frac{1}{2}\int h_x^2\, dx\right)^{-1/2}, \qquad \beta[h] = A_0 - \alpha[h]\int h\, dx, \qquad (4.4)$$

$$\alpha'[h] = \frac{\alpha^3}{2\ell_0^2}h_{xx}, \qquad \beta'[h] = -\alpha'\int h\, dx - \alpha, \qquad I_k[h] = \int h^{-k}\, dx, \qquad (4.5)$$

$$\zeta[h] = I_2^2/(I_1 I_3), \qquad \zeta'[h] = \left(\frac{1}{I_1 h^2} - \frac{4}{I_2 h^3} + \frac{3}{I_3 h^4}\right)\zeta, \qquad (4.6)$$

$$F[h] = \zeta[h^*] + (\alpha - 1)^2/2 + \beta^2/2, \qquad h^* = \alpha h + \beta \qquad (4.7)$$

$$F'[h] = \alpha\zeta'[h^*] + \left(\int \zeta'[h^*]h\, dx\right)\alpha' + \left(\int \zeta'[h^*]\, dx\right)\beta' + (\alpha - 1)\alpha' + \beta\beta' \qquad (4.8)$$

using a 30 point Gaussian quadrature rule on each spline segment to compute the integrals to machine precision. We use Nocedal's limited memory BFGS package (freely available from NetLib) to minimize $f(q)$, which is a quasi-Newton line search method which builds an approximate Hessian incrementally from the history of gradients $g(q)$ it has evaluated (Nocedal & Wright 1999). For n up to 256, we don't use the limited memory feature of the algorithm; for $n > 256$, we limit the number of Hessian update columns to 256. In practice, we actually define $h_q = 1/\sum q_i\varphi_i$ to prevent the BFGS algorithm from doing an agressive line search which causes h to become negative.

We now describe our choice of spline knots and the starting guess we use on the first pass of the algorithm (i.e. on the coarsest grid). The solution requires more resolution in the region where $h(x)$ is close to zero because this is where the curvature is highest, and because the integrals I_k involve negative powers of h. We use the interval $[-1/2, 1/2]$ as the computational domain and choose a knot spacing which is clustered at the origin:

$$x_i = \begin{cases} -3(i/n - 1/2)^2 - 2(i/n - 1/2)^3 & i = 0, 1, \ldots, n/2, \\ 3(i/n - 1/2)^2 - 2(i/n - 1/2)^3 & i = n/2, \ldots, n. \end{cases} \qquad (4.9)$$

Since the Euler-Lagrange equation (3.6) is invariant under translation $x \to x + a$ and reflection $x \to -x$, solutions will be translationally invariant and symmetric about their

extrema. Our goal is to find the solution (among all translations) which has a minimum at $x = 0$, where the resolution of the grid is highest. Suppose h is an even function. Since $F'[h]$ in (4.8) depends on x only through its dependence on h and h_{xx}, it will also be an even function of x. Since the knots are symmetric about the origin, the same is true at the discrete level: if $q_{n/2+i} = q_{n/2-i}$ for $1 \le i < n/2$, then the gradient g also has this property. The BFGS Hessian update formula (Nocedal & Wright 1999) respects this symmetry, hence by choosing a starting vector q such that h_q is symmetric about $x = 0$ and has a minimum there, we expect the final answer (and intermediate line search results) to have this property as well. Numerical roundoff can cause a slight drift in symmetry in the last few digits of the solution, but each time we refine the mesh, we symmetrize the solution before using it as a starting guess; on the finest meshes (when the starting guess is very good), the solution tends to be exactly symmetric in spite of roundoff error. On the first iteration, we evaluate the function $\tilde{h}(x) = A_0 - \ell_0/\sqrt{6} + \sqrt{6}\ell_0(|x| - x^2)$ at the knots and set $h(x) = \sum \tilde{h}(x_i)B_i(x)$, i.e. we use B-splines to smooth out a vertical translation of the critical parabola discussed in Section 3 and use it for the initial guess.

Figure 5 shows an example of a solution computed as described in this section for $\ell_0 = 0.32$, $A_0 = 1.2\ell_0/\sqrt{6}$. Although the variational derivative $F'[h]$ is not identically zero, this is the best possible solution in this spline space: the norm of the discrete gradient g in (4.2) is approximately 10^{-9}. As we refine the mesh, the true solution becomes better approximated by spline functions and $F'[h]$ converges to zero. The relative error in the computed swimming speed (using $c = 1.03017842643553$ obtained from the ODE method of Section 4.2 as a benchmark) and the number of iterations the BFGS algorithm required in order to converge is given in the following table:

n	relative error	function evaluations	
64	4.2×10^{-7}	306	
128	5.0×10^{-9}	178	
256	7.3×10^{-11}	82	
512	1.3×10^{-12}	50	
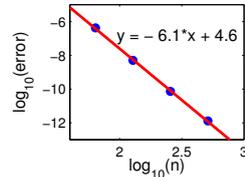
The 6th order convergence rate is a result of quadratic clustering of nodes near the origin. The entire computation took approximately 2 seconds on a 2.4 GHz desktop machine. When A_0 is closer to $A_{\mathrm{crit}} = \ell_0/\sqrt{6}$ and the solution is more sharply cusped at the origin, the number of iterations required by the BFGS algorithm can increase into the tens of thousands, causing the computation to take minutes to hours. By contrast, the method in Section 4.2 continues to require only a few seconds to run, and is able to maintain accuracy for A_0 much closer to A_{crit}.

Problem 2 (maximize efficiency). We now turn our attention to optimizing efficiency, defined the ratio of swimming speed to the power required to swim at that speed. As described in Section 3, $c/P = 1/(2I_1)$; hence, we wish to minimize I_1 (subject to area and arclength constraints) in order to maximize efficiency. We seek the global minimizer of the function

$$F[h] = I_1[\alpha h + \beta] + (\alpha - 1)^2/2 + \beta^2/2, \tag{4.10}$$

where α and β remain defined as in (4.4). Using the formula (3.8) for $F'[h]$ and proceeding as in Problem 1, we discover that the optimal discrete solution (in the spline space) is very nearly equal to the constant function $h(x) = A_0$, with the exception of a few high frequency oscillations to lengthen the curve and satisfy the arclength constraint (see
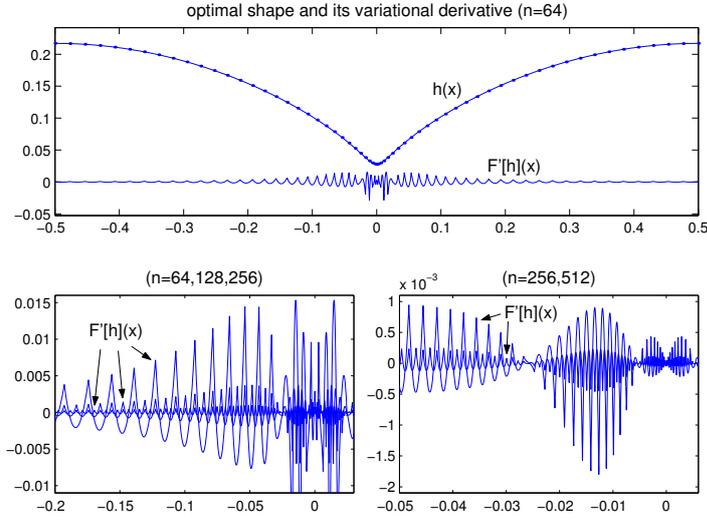
FIGURE 5. Top: solution obtained by direct minimization using periodic splines with 64 knots ($\ell_0 = 0.32$, $A_0 = 1.2\ell_0/\sqrt{6}$). Bottom: the variational derivative of the optimal solution in the spline space converges to zero as the grid is refined.
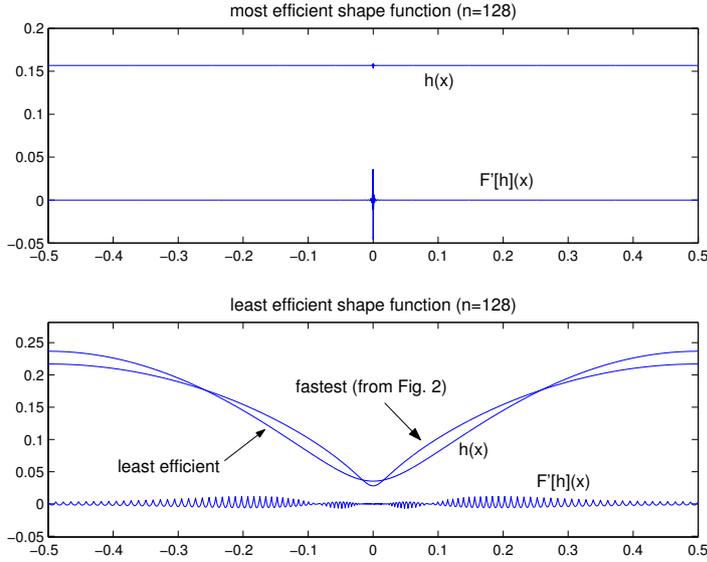

FIGURE 6. Top: the most efficient shape function ($\ell_0 = 0.32$, $A_0 = 1.2\ell_0/\sqrt{6}$) in the spline space is as close to a constant as possible without violating the constraints. There is no solution in the mesh refinement limit. Bottom: the least efficient wave profile is flatter near its minimum than the fastest profile for the same ℓ_0, A_0.

Figure 6). This can be understood as follows. By Jensen's inequality,

$$I_1 = \int_0^1 h(x)^{-1}\,dx \geq \left(\int_0^1 h(x)\,dx \right)^{-1} = A_0^{-1}. \tag{4.11}$$

It can be shown that any minimizing sequence h_k (such that $I_1[h_k] \to A_0^{-1}$) which satisfies the constraints (3.1) converges uniformly to the constant function $h(x) = A_0^{-1}$. Since we

assume $\ell_0 > 0$, this limiting function violates the arclength constraint and there is no optimal solution. Moreover, in order to approach the optimal efficiency $c/P = A_0/2$, the swimming speed c must approach zero; this is because a function h which is uniformly close to the constant function A_0 will satisfy $I_k \approx A_0^{-k}$, hence $\zeta = I_2^2/(I_1 I_3) \approx 1$ and $c = 6(1 - \zeta)/(4 - 3\zeta) \approx 0$. Interestingly, if we change the sign of I_1 in (4.10), we find there is a well defined "least efficient" swimmer; see Figure 6. Solutions to the Euler-Lagrange equation (3.9) actually solve this problem rather than the problem we intended to solve. We remark that Jensen's inequality also implies that the denominator of (3.9) is strictly positive for any non-constant positive function h; however, if h comes close to maximizing efficiency by approaching the constant function $h(x) = A_0$, the denominator tends to zero.

4.2. *Solving the Euler-Lagrange Equations via ODE Methods*

Problem 1 (maximize speed). In this section we use a Levenberg-Marquardt method (Nocedal & Wright 1999) to vary the parameters I_k and the initial condition $h(0) = b$ in the Euler-Lagrange equation

$$h_{xx} = f(h, I) := \left(\frac{2\ell_0^2}{A_0} \right) \left(\frac{h^{-2}/I_1 - 4h^{-3}/I_2 + 3h^{-4}/I_3}{I_2/I_1 - 4I_3/I_2 + 3I_4/I_3} - 1 \right) \tag{4.12}$$

until the solution is periodic, the constraints are satisfied, and the integrals of the solution match the parameters. More precisely, given the vector

$$q = (b, I_1, I_2, I_3, I_4) \in \mathbb{R}^5, \tag{4.13}$$

we define the function $h_q(x)$ as the solution of the ordinary differential equation (4.12) with initial conditions $h_q(0) = b$, $h_q'(0) = 0$. We then use Minpack (which is freely available from Netlib and employs a Levenberg-Marquardt method) to solve the nonlinear system of equations $r(q) = 0$, where

$$r_{\{k=1,2,3\}} = \frac{2}{I_k} \int_0^{\frac{1}{2}} h_q^{-k} \, dx - 1, \qquad r_4 = \frac{2}{A_0} \int_0^{\frac{1}{2}} h_q \, dx - 1, \qquad r_5 = h_q'(1/2). \tag{4.14}$$

Since (4.12) is invariant under translation $x \to x + a$ and reflection $x \to -x$, its solutions are symmetric about their extrema and all critical points are extrema; therefore, requiring that $h'(0) = 0$ and $r_5 = h'(1/2) = 0$ is equivalent to enforcing periodicity via $h(1) = h(0)$ and $h'(1) = h'(0) = 0$. The remaining two conditions $\frac{1}{2} \int_0^1 h_x^2 \, dx = \ell_0^2$ and $\int_0^1 h^{-4} \, dx = I_4$ are satisfied automatically, which can be seen by integrating (4.12) and its product with h from 0 to 1 and using periodicity.

To compute $h_q(x)$ and the integrals (4.14) numerically, we choose a coarse partition $0 = \tilde{x}_0 < \tilde{x}_1 < \cdots < \tilde{x}_M = 1/2$ of the interval $[0, 1/2]$ and set $\Delta_j = \tilde{x}_{j+1} - \tilde{x}_j$ for $j = 0, \ldots, M - 1$. We choose the $\tilde{x}_j$ so that the distribution of nodes is densest near the origin, as explained below. We then define $\{\theta_k, \tilde{w}_k\}_{k=1}^K$ to be the abscissas and weights of the K point Gaussian quadrature rule (Abramowitz & Stegun 1972) on the unit interval and use them to construct a finer partition with integration weights:

$$\begin{aligned} x_0 &= 0, & w_0 &= 0, & & \\ x_{jK+k} &= \tilde{x}_j + \theta_k \Delta_j, & w_{jK+k} &= \tilde{w}_k \Delta_j, & (0 \le j < M, \ 1 \le k \le K) & \\ x_n &= 1/2, & w_n &= 0, & (n = MK + 1). & \end{aligned} \tag{4.15}$$

We use fourth order Runge-Kutta (RK4) Hairer *et al.* (2000) to evaluate h_q at each node x_i and compute the integrals in (4.14) discretely, e.g. $r_2 = \frac{2}{I_k} \sum_{i=0}^n h_q(x_i)^{-2} w_i - 1$. Thus, it is not difficult to evaluate the function $r(q)$ on $\mathbb{R}^5$ numerically.

In order to use the Levenberg-Marquardt method, we must also be able to compute the Jacobian $J = \nabla r$. Let us define the functions

$$g_0(x) = \frac{\partial}{\partial b} h_q(x), \qquad g_{\{k=1,2,3,4\}} = \frac{\partial}{\partial I_k} h_q(x). \qquad (4.16)$$

It is well known (Coddington & Levinson 1984) that since h_q (denoted h from now on) satisfies the equation $h'' = f(h, I)$, the g_k satisfy the linear equations

$$g_0'' = \frac{\partial f}{\partial h}(h, I) g_0, \qquad\qquad g_0(0) = 1, \quad g_0'(0) = 0, \qquad (4.17)$$

$$g_k'' = \frac{\partial f}{\partial h}(h, I) g_k + \frac{\partial f}{\partial I_k}(h, I) \qquad g_k(0) = 0, \quad g_k'(0) = 0. \qquad (4.18)$$

Numerically, we compute g_0, g_k at the nodes x_i using $RK4$ to solve the equations (4.17), (4.18). This actually requires values of h at the half nodes $x_{i+1/2} = (x_i + x_{i+1})/2$, so we include these nodes when computing h via RK4 (but ignore them when computing the integrals in (4.14)). We then have

$$J = \begin{pmatrix} 2\int_0^{1/2} \begin{pmatrix} -1/I_1 h(x)^2 \\ -2/I_2 h(x)^3 \\ -3/I_3 h(x)^4 \\ 1/A_0 \end{pmatrix} [g_0(x), \dots, g_4(x)] \; dx \\ [g_0'(1/2), g_1'(1/2), g_2'(1/2), g_3'(1/2), g_4'(1/2)] \end{pmatrix} + \begin{pmatrix} 0 & a_1 & 0 & 0 & 0 \\ 0 & 0 & a_2 & 0 & 0 \\ 0 & 0 & 0 & a_3 & 0 \\ 0 & 0 & 0 & 0 & 0 \\ 0 & 0 & 0 & 0 & 0 \end{pmatrix}$$

where $a_k = -(2/I_k^2)\int_0^{1/2} h^{-k}\, dx$ and all integrals are carried out numerically using the weights w_i. Both $r(q)$ and $J(q)$ are inexpensive to compute, requiring only $O(n)$ operations to solve the relevant ODE's and compute the integrals. Since the Levenberg-Marquardt method is quadratically convergent when used to solve linear equations (as opposed to overconstrained least squares problems), very few iterations (typically 8-30) are required to converge to the solution as long as a good initial guess is known in advance. Therefore, when a guess is available (e.g. via extrapolation in a parameter study), the method is extremely efficient, requiring only a second or two even in the most ill-conditioned cases presented below.

We used this method to study the behavior of the swimming sheet as the area constraint A_0 approaches the critical value ($A_{\mathrm{crit}} = \ell_0/\sqrt{6}$) at which the sheet can touch the wall. We ran 201 trials with the constraints $\ell_0 = 0.32$, $A_0 = (1 + \delta)A_{\mathrm{crit}}$, where δ ranged from $\delta_0 = 0.2$ to $\delta_{200} = 9.945 \times 10^{-8}$ via the recursion $\delta_{k+1} = 0.93\delta_k$. We used $K = 20$ Gaussian quadrature points and $M = 300$ coarse gridpoints throughout the computation (for a total of $n + 1 = 6002$ nodes x_i). The spacing of the coarse grid points was chosen to be appropriately dense near the origin to resolve the behavior of the solution there. Originally we used $\tilde{x}_j = 3(j/2M)^2 - 2(j/2M)^3$, but after the scaling of the solution became clear, we switched to $\Delta_j = Ae^{j\alpha}$, where α is chosen so that $\frac{\Delta_{n-1}}{\Delta_0} = 50/(\delta \log(4.5/\delta))$ and A is chosen so that $\sum_{j=0}^{M-1} \Delta_j = 0.5$. Both choices for the $\tilde{x}_j$ work well, but the latter gives a more gradual transition from the finest spacing to the coarsest and does not require that we increase M over the range of δ studied here. On the first and second iteration, we used the method of Section 4.1 to compute a starting guess for $q = (b, I_{\{1,2,3,4\}})$. After that, we used logarithmic extrapolation to obtain the starting guess, e.g. $b_{k+1} = \exp[2\log(b_k) - \log(b_{k-1})]$.

The results of this study are summarized in Figure 7. The upper left plot shows that the optimal curves $h_k(x)$ do indeed approach the parabola $h_{\mathrm{crit}}(x) = \sqrt{6}\ell_0(|x| - x^2)$ as $\delta_k \to 0$ and $(A_0)_k \to A_{\mathrm{crit}}$. The plot on the right shows how the power $P = 2I_1 c$ and shape parameter $\zeta = I_2^2/(I_1 I_3)$ depend on δ_k. Recall that the swimming speed c is
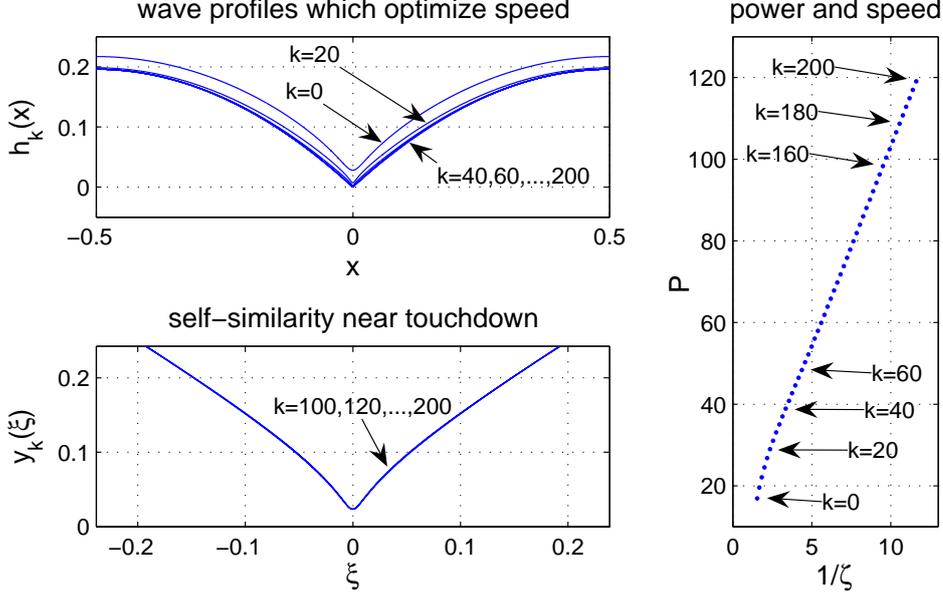
FIGURE 7. Upper left: the optimal curves $h_k(x)$ approach the periodic parabola $\sqrt{6}\ell_0(|x| - x^2)$ as $\delta_k \to 0$. Lower left: the curves appear to be self-similar when scaled as in (4.19). Right: as $\delta_k \to 0$, the swimming speed $c \approx \frac{3}{2} - \frac{3}{8}\zeta$ approaches 1.5 while the power required to swim at that speed grows without bound.

related to ζ via $c = 6(1 - \zeta)/(4 - 3\zeta)$, so for small ζ we have $c \approx \frac{3}{2} - \frac{3}{8}\zeta$. This plot shows that the power required to swim eventually grows linearly with ζ^{-1}, and diverges as the swimming speed approaches $c = 1.5$. We also find that solutions are self-similar near touchdown when rescaled by

$$y_k(\xi) = \frac{1}{\delta_k \log(2.75/\delta_k)} h_k\big(\delta_k \log(4.5/\delta_k)\xi\big). \tag{4.19}$$

The profiles correspond to one another for $100 \le k \le 200$ (or equivalently, for $1.4 \times 10^{-4} \ge \delta_k \ge 1.0 \times 10^{-7}$) to within one percent over the range of ξ shown in Figure 7. Because the x- and y-axes are both re-scaled via $\delta |\log \delta|$, the weighted averages E_k/I_k, J_k/I_k, etc. in (A 23)–(A 26) and (A 31)–(A 33) do not blow up as $\delta \to 0$. Hence, the lubrication approximation remains valid in the sense that the higher order corrections can be made arbitrarily small in comparison to the zeroth order terms (uniformly in δ) by a single choice of H/W (see Figure 8). We note that $P^{(0)}$ and $P^{(2)}$ both diverge due to the factor of I_1 in (A 31) and (A 32), but the latter is dominated by the former.

Problem 3 (maximize efficiency for a given swimming speed). We now turn to the problem of optimizing efficiency when both the arclength and speed are constrained. We could also constrain the volume by a trivial modification of the method presented below, but it seems more interesting to find the optimal volume as part of the solution rather than imposing a sub-optimal volume as a constraint. Reasoning as in Section 3, we arrive at the Euler-Lagrange equation

$$h_{xx} = -\frac{\lambda_1}{h^2} - \frac{\lambda_2}{h^3} + \frac{\lambda_3}{h^4} \tag{4.20}$$
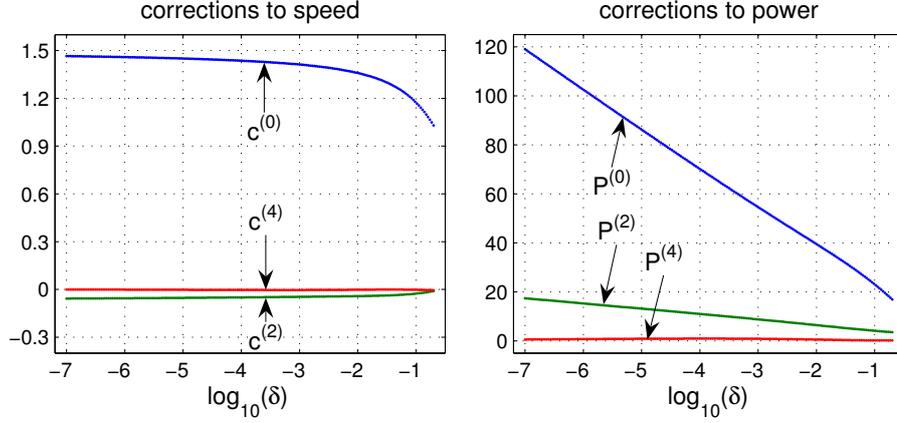
FIGURE 8. Plots of the expansion coefficients for speed $c = c^{(0)} + (H/W)^2 c^{(2)} + (H/W)^4 c^{(4)} + \cdots$ and power $P = P^{(0)} + (H/W)^2 P^{(2)} + (H/W)^4 P^{(4)} + \cdots$. Since the higher order coefficients remain small in comparison to $c^{(0)}$ and $P^{(0)}$, the lubrication approximation appears to remain valid as the constrained area $A_0 = (1 + \delta)A_{\text{crit}}$ approaches $A_{\text{crit}} = \ell_0/\sqrt{6}$.

with constraints

$$\frac{1}{2} \int_0^1 h_x^2 \, dx = \ell_0^2, \qquad \frac{I_2^2}{I_1 I_3} = \zeta_0, \qquad 3\lambda_2 I_2 = 4\lambda_3 I_3. \qquad (4.21)$$

In contrast to the approach described for Problem 1 above, the I_k are now treated as functionals of h rather than as parameters in the equation which must be varied until the equality $I_k = \int h^{-k} \, dx$ holds. The parameters λ_k in (4.20) turn out to be positive numbers. Given the vector

$$q = (b, \lambda_1, \lambda_2, \lambda_3) \in \mathbb{R}^4 \qquad (4.22)$$

we define the function $h(x)$ as the solution of the ODE (4.20) with initial conditions $h(0) = b$, $h'(0) = 0$ and use Minpack to solve the nonlinear system of equations $r(q) = 0$, where

$$r_1 = \int_0^{\frac{1}{2}} h_x^2 \, dx - \ell_0^2, \quad r_2 = \frac{I_2^2}{I_1 I_3} - \zeta_0, \quad r_3 = \frac{\lambda_2 I_2}{\lambda_3 I_3} - \frac{4}{3}, \quad r_4 = h'(1/2) \qquad (4.23)$$

and $I_k = 2 \int_0^{1/2} h^{-k} \, dx$. The Jacobian $J = \nabla r$ is given by

$$J = \left(2 \int_0^{1/2} \begin{pmatrix} h_x \frac{\partial}{\partial x} \\ \frac{I_2^2}{I_1 I_3} \left[\frac{1}{I_1 h^2} - \frac{4}{I_2 h^3} + \frac{3}{I_3 h^4} \right] \\ \frac{3\lambda_2 I_2}{\lambda_3 I_3^2 h^4} - \frac{2\lambda_2}{\lambda_3 I_3 h^3} \end{pmatrix} [g_0, \ldots, g_3] \, dx \\ [g_0'(1/2), g_1'(1/2), g_2'(1/2), g_3'(1/2)] \right) + \begin{pmatrix} 0 & 0 & 0 & 0 \\ 0 & 0 & 0 & 0 \\ 0 & 0 & a & b \\ 0 & 0 & 0 & 0 \end{pmatrix}$$

where $a = I_2/\lambda_3 I_3$, $b = -\lambda_2 I_2/\lambda_3^2 I_3$, and the functions $g_0(x) = \frac{\partial}{\partial b} h(x)$, $g_{\{k=1,2,3\}} = \frac{\partial}{\partial \lambda_k} h(x)$ satisfy equations analogous to (4.17), (4.18) above. We compute $r(q)$ and $J(q)$ numerically just as before, using a fourth order Runge-Kutta scheme to evaluate $h(x)$ and $g_k(x)$ at nodes which are appropriately spaced to compute the integrals via gaussian quadrature rules.

We used this method to study the behavior of the swimming sheet as the swimming speed c approaches its maximal value $3/2$. We ran 101 trials with the constraints $\ell_0 = 0.32$
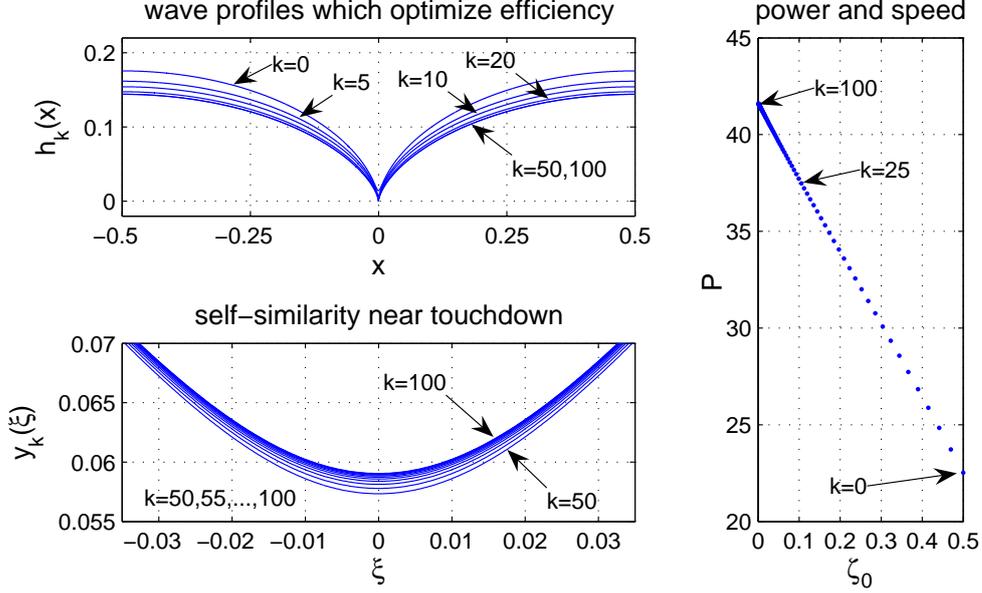
FIGURE 9. Top left: the optimal curves $h_k(x)$ approach a limiting curve with a cusp at the origin. Right: unlike the area constrained problem, the power $P = 2I_1c$ remains bounded as the speed $c \approx \frac{3}{2} - \frac{3}{8}\zeta_0 \to 3/2$. Bottom left: the curves y_k appear to be self-similar as $\delta_k \to 0$ when scaled as in (4.24). In the region shown, y_{100} differs from y_{50} by about 3% and from y_{95} by about 0.05%. If we zoom out, we find that y_{100} differs from y_{50} by less than 1% over the range $0.05 \leq |\xi| \leq 200$. The scaling of the x-axis in this plot varies from $\delta_{50}^3 = 1.12 \times 10^{-5}$ to $\delta_{100}^3 = 1.00 \times 10^{-9}$.

and $\zeta_0 = \delta$, where δ ranged from $\delta_0 = 0.5$ to $\delta_{100} = 0.001$ via the recursion $\delta_{k+1} = 0.94\delta_k$. To fully resolve the solution near the origin without using an excessive number of gridpoints, we used an exponentially graded coarse grid spacing $\Delta_j = Ae^{j\alpha}$, where α was chosen so that $\frac{\Delta_{n-1}}{\Delta_0} = 10\delta^{-3}$ and A was chosen so that $\sum_{j=0}^{M-1} \Delta_j = 0.5$. We used $K = 20$ Gaussian quadrature points and $M = 300$ coarse gridpoints throughout the computation (for a total of 6002 nodes x_i). On the first iteration, we experimented with q by hand until the curve h had a maximum near $1/2$ and let Minpack run through a few thousand trust region searches until it found the nearest solution satisfying $r(q) = 0$. On the second iteration, we used the result of the first iteration as a starting guess. On all further iterations, we used logarithmic extrapolation to obtain the new starting guess, e.g. $b_{k+1} = \exp[2\log(b_k) - \log(b_{k-1})]$. The number of trust region searches was typically between 10 and 30, with a few exceptions in the hundreds. The running time of the entire parameter study was around one minute on a 2.4 GHz desktop machine.

The results of this study are summarized in Figure 9. Through trial and error, we discovered that the solutions are self-similar near the origin in the sense that the re-scaled functions

$$y_k(\xi) = \frac{1}{\delta_k^2} h_k \left(\delta_k^3 \xi \right) \tag{4.24}$$

converge to a common curve as $\delta_k \to 0$. This suggests that the cusp in the limiting curve in the upper left plot is asymptotically of the form $\alpha|x|^{2/3}$, which has a finite first negative moment I_1 in the power formula $P = 2I_1c$. By contrast, I_1 is infinite for the limiting curve $\sqrt{6}\ell_0(|x| - x^2)$ of Problem 1 above. Unfortunately, this cusp also causes
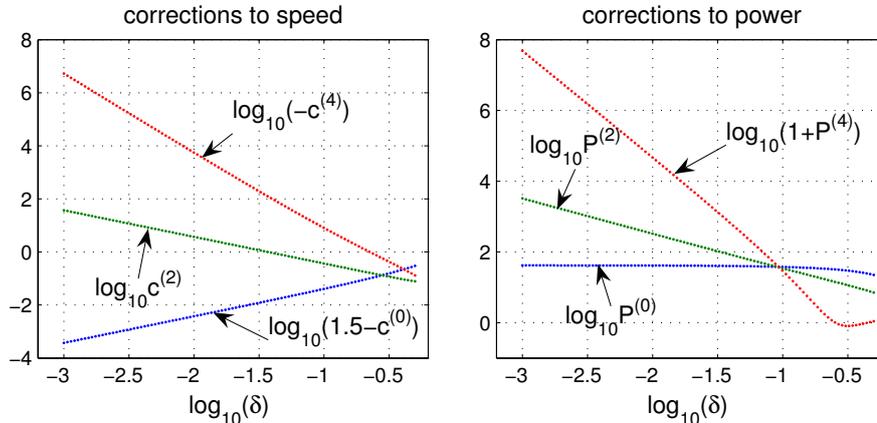
FIGURE 10. Plots of the expansion coefficients for speed and power. In contrast to Problem 1, the higher order coefficients grow without bound as $\delta \to 0$ while the zeroth order coefficients remain bounded; hence the lubrication approximation cannot be used to study the critical limit $\delta \to 0$. Since $c^{(2)}$ is large and positive, it is an interesting question whether the speed c can actually exceed $3/2$. It turns out that $-c^{(4)}$ is large enough to prevent this at the 4th order approximation, however the question remains open for the full Stokes equations.

the weighted averages E_k/I_k, J_k/I_k, etc. in the expansion coefficients (A 23)–(A 26), (A 31)–(A 33) to diverge in the limit as $\delta = \zeta_0 \to 0$ (see Figure 10). This problem can be superficially overcome by allowing H/W to depend on δ; for example, if we set $H = H_0\delta$ and expand in powers of H_0/W instead of H/W, we find that the expansion coefficients $\delta^2 c^{(2)}$, $\delta^2 P^{(2)}$, $\delta^4 c^{(4)}$, $\delta^4 P^{(4)}$ approach zero as $\delta \to 0$. Multiplying H_0/W by δ flattens out the optimal curves enough to prevent infinite slopes from developing in this limit. The price we pay for this remedy is that the relationship between physical power and dimensionless power depends on H/W. By decreasing H/W in order to stay within the lubrication regime, we are destroying the key feature of the solution, namely that the power remains bounded as $\delta \to 0$. Therefore we suggest, to properly study this limit, one must go beyond the lubrication approximation by including higher order terms in the objective function or working directly with the full Stokes equations.

5. Discussion

In this study, we have presented the first steps in optimizing low Reynolds number swimmers activated at the surfaces of thin films. It is hoped that these results can be used as guidelines in designing efficient mechanical swimmers and crawlers as well as increase our understanding of biological systems. The latter, understanding optimization in biology, is a much more ambitious goal as appropriate cost functions, which can often be well-defined in engineering systems, are not at all obvious in biological counterparts. Furthermore, in optimizing mechanical shapes, we have only scratched the surface of the space of relevant parameters; equally relevant questions, such as optimizing material properties of the fluid, remain largely unexplored.

It is also worth emphasizing the somewhat surprising success of the lubrication approximation even in the limit of fairly sharp profiles. In fact, the profiles resulting from maximizing speed, a criteria that is likely to be relevant for some microorganisms in environments where there is an abundance of energy at small scales, remain within the limits of validity of the lubrication approximation.

However, we have also demonstrated that some care must be taken as the success of the lubrication analysis is tied to the optimal membrane shape which in turn depends on the choice of the cost function. For certain cost functions (e.g. efficiency at a given speed), one may need to solve full Stokes' problem depending on the sharpness of the optimal profiles near touchdown. While all of the analysis herein has been done in the lubrication limit, we believe that direct minimization method using cubic splines can be generalized to solve the shape optimization problem for the full Stokes' equations in the non-lubrication regime, but this is work in progress.

REFERENCES

ABRAMOWITZ, M. & STEGUN, I. A., ed. 1972 *Handbook of Mathematical Functions with Formulas, Graphs, and Mathematical Tables*, 9th edn. New York: Dover Publications, Inc.

CARL DE BOOR 2001 *A Practical Guide to Splines*, reprint edn. New York: Springer.

CAI, Z., MANTEUFFEL, T. A. & MCCORMICK, S. F. 1997 First-order system least squares for the Stokes equations, with application to linear elasticity. *SIAM J. Numer. Anal.* **34** (5), 1727–1741.

CAMACHO-LOPEZ, M., FINKELMANN, H., PALFFY-MUHORAY, P. & SHELLEY, M. 2004 Fast liquid-crystal elastomer swims into the dark. *naure materials* **3**, 307 – 310.

CHAN, B., BALMFORTH, N. J. & HOSOI, A. E. 2005 Building a better snail: Lubricaiton and adhesive locomotion. *Phys. Fluids* **17** (11), 113101.

CODDINGTON, E. A. & LEVINSON, N. 1984 *Theory of Ordinary Differential Equations*. Malabar, Florida: Krieger Publishing Company.

DENNY, M. W. 1980 The role of gastropod pedal mucus in locomotion. *Nature* **285**, 160.

DILUZIO, W. R., TURNER, L., MAYER, M., GARSTECKI, P., WEIBEL, D. B., BERG, H. C. & WHITESIDES, G. M. 2005 *Escherichia coli* swim on the right-hand side. *Nature* **435**, 1271 – 1274.

HAIRER, E., NORSETT, S. P. & WANNER, G. 2000 *Solving Ordinary Differential Equations I: Nonstiff Problems*, 2nd edn. Berlin: Springer.

HANCOCK, G. J. 1953 The self-propulsion of microscopic organisms through liquids. *Proc. Roy. Soc. London A* **217** (1128), 96 – 121.

LAUGA, E., DILUZIO, W. R., WHITESIDES, G. M. & STONE, H. A. 2006 Swimming in circles: Motion of bacteria near solid boundaries. To appear in Biophys. J.

LIGHTHILL, J. 1976 Flagellar hydrodynamics: The John von Neumann lecture, 1975. *SIAM Review* **18** (2), 161 – 230.

NOCEDAL, J. & WRIGHT, S. J. 1999 *Numerical Optimization*. New York: Springer.

PEDLEY, T. J. & KESSLER, J. O. 1992 Hydrodynamic phenomena in suspensions of swimming microorganisms. *Ann. Rev. Fluid Mech.* **24**, 313 – 358.

REYNOLDS, O. 1886 On the theory of lubrication and its applications to Mr. Beauchamp Tower's experiments, including an experimental determination of the viscosity of olive oil. *Philos. Trans. R. Soc. London* **177**, 157.

TAYLOR, G. 1951 Analysis of swimming microscopic organisms. *Proc. Roy. Soc. London A* **209** (1099), 447 – 461.

VLÈS, F. 1907 Sur les ondes pediuses de mollosques reptateurs. *C. R. Hebd. Seances Acad. Sci.* **145**, 276.

Appendix A. Computing Expansion Solutions

We now describe our algorithm for computing higher order corrections to the lubrication approximation. Recall that the dimensionless variables are related to the physical variables via $\hat{x} = Wx$, $\hat{y} = Hy$, $\hat{h}(x) = Hh(x)$, $\hat{c}_i = Vc_i$, $\hat{\mathbf{u}} = V\mathbf{u}$, $\hat{p} = \frac{\mu V W}{H^2}p$, $\hat{P} = \mu V \frac{W}{H}P$, and $\hat{F} = \mu V \frac{W}{H}F$. We expand all variables in powers of H/W, e.g.

$$u(x,y) = u^{(0)}(x,y) + \tfrac{H}{W}u^{(1)}(x,y) + \left(\tfrac{H}{W}\right)^2 u^{(2)}(x,y) + \cdots, \qquad (A\,1)$$

and match like powers of H/W in the equations. The incompressibility condition $v_y = -\frac{H}{W}u_x$ gives

$$v_y^{(0)} = 0, \qquad v_y^{(k)} = -u_x^{(k-1)}, \qquad (k \geq 1), \qquad (A\,2)$$

while the momentum equations $p_y = \left(\frac{H}{W}\right)^3 v_{xx} + \frac{H}{W}v_{yy}$ and $p_x = \left(\frac{H}{W}\right)^2 u_{xx} + u_{yy}$ yield

$$p_y^{(0)} = 0, \qquad p_y^{(1)} = v_{yy}^{(0)}, \qquad p_y^{(2)} = v_{yy}^{(1)}, \qquad p_y^{(k)} = v_{xx}^{(k-3)} + v_{yy}^{(k-1)}, \qquad (k \geq 3), \qquad (A\,3)$$

$$u_{yy}^{(0)} = p_x^{(0)}, \qquad u_{yy}^{(1)} = p_x^{(1)}, \qquad\qquad\qquad u_{yy}^{(k)} = p_x^{(k)} - u_{xx}^{(k-2)}, \qquad (k \geq 2). \qquad (A\,4)$$

The boundary condition $(u,v) = c_1(1, \frac{H}{W}h_x)[1 + \left(\frac{H}{W}\right)^2 h_x^2]^{-1/2}$ on Γ_1 becomes

$$u^{(0)} = c_1, \qquad u^{(2)} = -\frac{c_1}{2}h_x^2, \qquad u^{(4)} = \frac{3}{8}c_1 h_x^4, \qquad u^{(2k)} = c_1 \binom{-1/2}{k} h_x^{2k}, \qquad (A\,5)$$

$$v^{(1)} = c_1 h_x, \qquad v^{(3)} = -\frac{c_1}{2}h_x^3, \qquad v^{(5)} = \frac{3}{8}c_1 h_x^5, \qquad v^{(2k+1)} = c_1 \binom{-1/2}{k} h_x^{2k+1}, \qquad (A\,6)$$

with all other terms equal to zero. Similarly, on Γ_2 we have

$$u^{(0)} = c_2, \quad v^{(0)} = 0, \qquad u^{(k)} = 0, \quad v^{(k)} = 0, \qquad (k \geq 1). \qquad (A\,7)$$

The zeroth order terms were computed in Section 2.2 above. We note that (A 2) and the boundary conditions (A 6), (A 7) imply that $v^{(0)} = 0$. To compute $v^{(1)}$, we use (A 2) and (A 7) to conclude that

$$v^{(1)}(x,y) = -\int_0^y u_x^{(0)}(x,\eta)\,d\eta. \qquad (A\,8)$$

The boundary condition (A 6) is satisfied because $Q^{(0)} = \int_0^h u^{(0)}(x,y)\,dy$ is a constant:

$$0 = \frac{\partial Q^{(0)}}{\partial x} = \int_0^h u_x^{(0)}(x,y)\,dy + u^{(0)}(x,h(x))h'(x) = -v^{(1)}(x,h(x)) + c_1 h'(x). \qquad (A\,9)$$

The variables $p^{(1)}$ and $u^{(1)}$ satisfy identical equations to $p^{(0)}$ and $u^{(0)}$, namely $p_y^{(1)} = 0$, $u_{yy}^{(1)} = p_x^{(1)}$, except the boundary conditions on $u^{(1)}$ are now zero. We may therefore repeat the zeroth order case with $c_1 = c_2 = 0$ to conclude that $p^{(1)} = \text{const}$, $u^{(1)} = 0$. An easy induction argument shows that $v^{(k)} = 0$ for k even and $p^{(k)} = \text{const}$, $u^{(k)} = 0$ for k odd. Moreover, when k is odd, $v^{(k)} = -\int_0^y u_x^{(k-1)}(x,\eta)\,d\eta$ and the boundary condition on the top wall may be checked by differentiating the constant $Q^{(k-1)} = \int_0^h u^{(k-1)}(x,y)dy$.

We now show how to compute $p^{(k)}$, $u^{(k)}$ when k is even. The main difference from the zeroth order case is that now $p^{(k)}$ depends on y as well as x. Integrating (A 3), we obtain

$$p^{(k)}(x,y) = q^{(k)}(x) + \int_0^y v_{xx}^{(k-3)}(x,\eta) + v_{yy}^{(k-1)}(x,\eta)\,d\eta \qquad (A\,10)$$

with $v_{xx}^{(k-3)}$ omitted when $k = 2$. The function $q^{(k)}(x)$ will be determined in the same way $p^{(0)}(x)$ was found in the lubrication analysis. First we solve the two point boundary value problem

$$u_{yy}^{(k)} = p_x^{(k)} - u_{xx}^{(k-2)}, \quad u^{(k)}(x,0) = 0, \quad u^{(k)}(x,h(x)) = c_1 \binom{-1/2}{k} h_x^{(2k)} \qquad (A\,11)$$

by integrating twice in the y direction: $u_y^{(k)}(x,y) = a + \int_0^y u_{yy}^{(k)}(x,\eta)\,d\eta$, $u^{(k)}(x,y) = \int_0^y u_y^{(k)}(x,\eta)\,d\eta$. The unknown constant a is chosen so that the boundary condition on

the top wall is satisfied. Keeping track of the coefficient in front of $q_x^{(k)}$ in this process, we find that

$$u^{(k)}(x,y) = \left(\frac{y^2}{2} - \frac{hy}{2}\right) q_x^{(k)}(x) + w^{(k)}(x,y), \qquad (A\,12)$$

where $w^{(k)}$ depends on x only through h and its derivatives. This last fact follows from the observation that higher order variables are obtained by differentiating and integrating lower order variables, and

$$u^{(0)}(x,y) = 6\left(\frac{y^2}{2} - \frac{hy}{2}\right)\left(\frac{c_1 + c_2}{h^2} - \frac{c_1 + c_2}{h^3}\frac{I_2}{I_3}\right) + \frac{y}{h}c_1 + \left(1 - \frac{y}{h}\right)c_2 \qquad (A\,13)$$

depends on x only through $h(x)$. For example, when $k = 2$, six of the twenty-two terms of $w^{(k)}(x,y)$ are

$$w^{(k)}(x,y) = 6(c_1 + c_2)\frac{I_2 y^4}{I_3 h^5}h_x^2 + \frac{c_1 + c_2}{3}y h_{xx} + (c_1 - 2c_2)\frac{2y^3}{3h^2}h_{xx} + \cdots. \qquad (A\,14)$$

Next we integrate (A 12) from 0 to h and solve for q_x:

$$q_x^{(k)}(x) = \frac{12}{h^3}\left(\int_0^h w^{(k)}(x,y)\,dy - Q^{(k)}\right). \qquad (A\,15)$$

Since the flux is a constant for any particular geometry in the full Stokes equations, each term $Q^{(k)}$ in its expansion in H/W must also be independent of x. Since $q^{(k)}$ is periodic, it's integral from 0 to 1 vanishes and we obtain

$$Q^{(k)} = \frac{1}{I_3}\int_0^1 \frac{1}{h^3}\int_0^h w^{(k)}(x,y)\,dy\,dx. \qquad (A\,16)$$

The most difficult part of the computation occurs here: we must find a way to have the computer algebra system (in our case Mathematica) convert all the integrals it encounters into appropriate symbols, e.g.

$$\int_0^1 \frac{1}{h^k}\,dx \to I_k, \quad \int_0^1 \frac{h_x^2}{h^k}\,dx \to E_k, \quad \int_0^1 \frac{h_x^4}{h^k}\,dx \to J_k, \quad \int_0^1 \frac{h^2 h_{xx}^2}{h^k}\,dx \to G_k, \quad (A\,17)$$

and so on. (These are all the integrals which arise through 4th order). We must also convert equivalent integrals into these symbols, e.g. $\int \frac{h_x^2 h_{xx}}{h^k}dx \to \frac{k}{3}J_{k+1}$. We do this by defining a list of conversion pairs $\{h[x]^{-1}, I_1, h'[x]^2/h[x], E1, \dots\}$, taking the coefficient of $\frac{1}{h^3}\int_0^h w^{(k)}(x,y)\,dy$ with respect the first member of each pair, multiplying it by the second member, and dividing by I_3 in the new expression for $Q^{(k)}$. Finally, once $Q^{(k)}$ is known, we obtain $q_x^{(k)}(x)$, $u^{(k)}(x,y)$ and $p^{(k)}(x,y)$ from (A 15), (A 13) and (A 10).

We now show how the higher order velocity and pressure fields may be used to compute corrections to the swimming speed and power. Non-dimensionalizing (2.9) and expanding in powers of $\varepsilon = H/W$, we obtain

$$F_0^{(0)}(c_1,c_2) = \int_{\Gamma_1} p_x^{(0)}h - u_y^{(0)}\,dx \qquad = \int_{\Gamma_2} -u_y^{(0)}\,dx, \qquad (A\,18)$$

$$F_0^{(2)}(c_1,c_2) = \int_{\Gamma_1} p_x^{(2)}h - u_y^{(2)} - h_x^2 u_y^{(0)}\,dx \qquad = \int_{\Gamma_2} -u_y^{(2)}\,dx, \qquad (A\,19)$$

$$F_0^{(4)}(c_1,c_2) = \int_{\Gamma_1} p_x^{(4)}h - u_y^{(4)} - h_x^2 u_y^{(2)}\,dx \qquad = \int_{\Gamma_2} -u_y^{(4)}\,dx. \qquad (A\,20)$$

Here p_x stands for $\frac{\partial}{\partial x}[p(x, h(x))]$ rather than $p_x(x, h(x))$ and the zero subscript is used to distinguish the expansion with c_2 held fixed from the expansion

$$F(c_1, c_2^{(0)} + \varepsilon^2 c_2^{(2)} + \varepsilon^4 c_2^{(4)} + \cdots) = F^{(0)} + \varepsilon^2 F^{(2)} + \varepsilon^4 F^{(4)} + \cdots. \qquad (A\,21)$$

The integrals in (A 18)–(A 20) are computed in the same way that $Q^{(k)}$ was computed, namely by running through the list of conversion pairs and replacing expressions involving the integrands in (A 17) by the corresponding symbols. To check for errors, we evaluate both formulas for $F_0^{(k)}$ to be sure they are equal. (This is how we noticed that a distinction must be made between $\partial_x[p(x, h(x))]$ and $p_x(x, h(x))$ when integrating by parts.) We now set $a_k = F_0^{(k)}(1, 0)$, $b_k = F_0^{(k)}(0, 1)$ so that by (2.3), with $\varepsilon = H/W$, we have

$$\frac{c_2}{c_1} = -\frac{F_1}{F_2} = -\frac{a_0 + \varepsilon^2 a_2 + \varepsilon^4 a_4 + \cdots}{b_0 + \varepsilon^2 b_2 + \varepsilon^4 b_4 + \cdots} = \frac{c_2^{(0)}}{c_1} + \frac{c_2^{(2)}}{c_1}\varepsilon^2 + \frac{c_2^{(4)}}{c_1}\varepsilon^4 + \cdots$$

$$= -\frac{a_0}{b_0} - \left(\frac{a_2}{b_0} - \frac{a_0 b_2}{b_0^2}\right)\varepsilon^2 - \left(\frac{a_4}{b_0} - \frac{a_2 b_2}{b_0^2} + \frac{a_0 b_2^2}{b_0^3} - \frac{a_0 b_4}{b_0^2}\right)\varepsilon^4 + \cdots. \qquad (A\,22)$$

These formulas for $c_2^{(k)}$ are equivalent to setting each term $F^{(k)}$ to zero in (A 21). In terms of the integrals (A 17), we obtain

$$c_2^{(0)} = -\frac{2 - 3\zeta}{4 - 3\zeta} c_1, \qquad (A\,23)$$

$$c_2^{(2)} = \frac{-c_1}{10(4 - 3\zeta)^2}\left[(8 + 10\zeta)\frac{E_1}{I_1} + 48\zeta\frac{E_3}{I_3} - (44\zeta + 15\zeta^2)\frac{E_2}{I_2}\right], \qquad (A\,24)$$

$$c_2^{(4)} = \frac{-c_1}{12600(4 - 3\zeta)^3}\left[(-10752 - 13440\zeta)\frac{E_1^2}{I_1^2} - 193536\zeta\frac{E_3^2}{I_3^2} + (-88704\zeta - 30240\zeta^2)\frac{E_1 E_3}{I_1 I_3} + \right.$$

$$(-16896 + 26112\zeta - 10080\zeta^2)\frac{G_1}{I_1} + (2304\zeta - 1728\zeta^2)\frac{G_3}{I_3} + (-14304 + 1488\zeta + 6930\zeta^2)\frac{J_1}{I_1} + (91392\zeta$$

$$+ 60480\zeta^2)\frac{E_1 E_2}{I_1 I_2} + (-82944\zeta + 62208\zeta^2)\frac{J_3}{I_3} + (177408\zeta + 254016\zeta^2)\frac{E_2 E_3}{I_2 I_3} + (-32256\zeta - 193536\zeta^2$$

$$\left. - 30240\zeta^3)\frac{E_2^2}{I_2^2} + (59344\zeta - 17208\zeta^2 - 20475\zeta^3)\frac{J_2}{I_2} + (23808\zeta - 38016\zeta^2 + 15120\zeta^3)\frac{G_2}{I_2}\right]. \qquad (A\,25)$$

Note that each term in these expansions is a weighted average; for example, $\frac{J_3}{I_3}$ is the average value of h_x^4 with respect to the weight function h^{-3}. Expanding the arclength $L = W\int_0^1 (1 + \varepsilon^2 h_x^2)^{1/2}\,dx = W(1 + \frac{\varepsilon^2}{2}E_0 - \frac{\varepsilon^4}{8}J_0 + \cdots)$ and using (2.4), we find

$$\frac{c}{c_1} = \frac{W}{L} - \frac{c_2}{c_1} = 1 - \frac{c_2^{(0)}}{c_1} + \left(-\frac{E_0}{2} - \frac{c_2^{(2)}}{c_1}\right)\varepsilon^2 + \left(\frac{E_0^2}{4} + \frac{J_0}{8} - \frac{c_2^{(4)}}{c_1}\right)\varepsilon^4 + \cdots. \quad (A\,26)$$

The new terms E_0, J_0 which arise due to the arclength correction may also be thought of as weighted averages with weight function 1; (note that $I_0 = 1$).

To compute corrections to the power, we non-dimensionalize (2.8) and expand in powers of $\varepsilon = H/W$:

$$P_0^{(0)}(c_1, c_2) = \int_{\Gamma_1} u_y^{(0)}\,dx, \qquad (A\,27)$$

$$P_0^{(2)}(c_1, c_2) = \int_{\Gamma_1} \left(u_y^{(2)} + \frac{3}{2}h_x^2 u_y^{(0)}\right)dx, \qquad (A\,28)$$

$$P_0^{(4)}(c_1, c_2) = \int_{\Gamma_1} \left(u_y^{(4)} + \frac{3}{2}h_x^2 u_y^{(2)} + \frac{3}{8}h_x^4 u_y^{(0)}\right)dx. \qquad (A\,29)$$

The subscript 0 is used to distinguish the expansion holding c_2 fixed from the one that

actually gives the corrections to the power required to swim:

$$P\left(c_1, c_2^{(0)} + \varepsilon^2 c_2^{(2)} + \varepsilon^4 c_2^{(4)} + \cdots\right) = P^{(0)} + \varepsilon^2 P^{(2)} + \varepsilon^4 P^{(4)} + \cdots$$
$$= c_1\left(\alpha_0 + \varepsilon^2\alpha_2 + \cdots\right) + \left(c_2^{(0)} + \varepsilon^2 c_2^{(2)} + \cdots\right)\left(\beta_0 + \varepsilon^2\beta_2 + \cdots\right), \quad \text{(A\,30)}$$

where $\alpha_k = P_0^{(k)}(1,0)$ and $\beta_k = P_0^{(k)}(0,1)$. The result of this computation is

$$P^{(0)} = \frac{12I_1(1-\zeta)}{4-3\zeta}c_1 = 2I_1 c, \tag{A\,31}$$

$$P^{(2)} = \frac{6I_1 c_1}{5(4-3\zeta)^2}\left[(8-10\zeta+5\zeta^2)\frac{E_1}{I_1} - (4\zeta+5\zeta^2)\frac{E_2}{I_2} + 8\zeta\frac{E_3}{I_3}\right], \tag{A\,32}$$

$$P^{(4)} = \frac{I_1 c_1}{1050(4-3\zeta)^3}\Big[(-8064\zeta-10080\zeta^2)\frac{E_1 E_3}{I_1 I_3} + (-672-1680\zeta-1050\zeta^2)\frac{E_1^2}{I_1^2} + (384\zeta-288\zeta^2)\frac{G_3}{I_3} +$$

$$(-13824\zeta+10368\zeta^2)\frac{J_3}{I_3} + (16128\zeta+52416\zeta^2)\frac{E_2 E_3}{I_2 I_3} + (-2016\zeta-23856\zeta^2-13230\zeta^3)\frac{E_2^2}{I_2^2} + (3824\zeta+$$

$$6232\zeta^2-6825\zeta^3)\frac{J_2}{I_2} + (6144-18048\zeta+16800\zeta^2-5040\zeta^3)\frac{G_1}{I_1} + (7392\zeta+11760\zeta^2+3150\zeta^3)\frac{E_1 E_2}{I_1 I_2} +$$

$$(-8544+15648\zeta-11550\zeta^2+3465\zeta^3)\frac{J_1}{I_1} + (8448\zeta-13056\zeta^2+5040\zeta^3)\frac{G_2}{I_2} - 32256\zeta\frac{E_3^2}{I_3^2}\Big]. \tag{A\,33}$$

Again we find that each term in the expansion (except for the overall factor of I_1) is a weighted average such as J_2/I_2 or E_3^2/I_3^2.